BELLCOMM, INC.
955 L'ENFANT PLAZA NORTH, S.W. WASHINGTON, D.C. 20024

COVER SHEET FOR TECHNICAL MEMORANDUM

TITLE- The Pointing Accuracy of an Orbiting Gimbal Mounted Telescope

TM-69-1022-2

DATE- February 17, 1969

FILING CASE NO(S)-620

AUTHOR(S)- P. G. Smith

FILING SUBJECT(S)-
(ASSIGNED BY AUTHOR(S)- Astronomy
Manned Space Flight
Attitude Control
Telescope Systems

ABSTRACT

We investigate the pointing accuracy obtainable with a control system of the type used on the Apollo Telescope Mount (ATM). It is shown that the current ATM design has a pointing error of less than 0.1 seconds of arc in the presence of crew motion and that the bulk of this error is due to so-called breakout torque in the gimbal torquers. Means are discussed for reducing breakout torque and other sources of error to the extent that pointing errors not exceeding .01 arc seconds are attainable with an ATM type system. Thus, such a system would meet the pointing requirements of a large (1 meter) diffraction-limited stellar telescope.

Results are obtained with the aid of two mathematical models that compute the telescope attitude response to crew motion disturbances, the latter being represented in terms of single motion force and moment time histories applied to specific space-craft locations; one of the models affords a simplified understanding of the error-producing phenomena, whereas the other model provides for three-dimensional, flexible body dynamics.

SEE REVERSE SIDE FOR DISTRIBUTION LIST

Table of Contents

BELLCOMM, INC.
955 L'ENFANT PLAZA NORTH, S.W. WASHINGTON, D. C. 20024

SUBJECT: The Pointing Accuracy of an Orbiting Gimbal Mounted Telescope

DATE: February 17, 1969

FROM: P. G. Smith

TM-69-1022-2

TECHNICAL MEMORANDUM

1.0 INTRODUCTION

1.1 Background

Large orbiting astronomical telescopes are potentially capable of diffraction-limited performance.* To realize this goal, however, it is often necessary to isolate the telescope from motions of the spacecraft that carries it. One means of providing rotational isolation is that of mounting the telescope to the spacecraft with a set of gimbals whose axes nominally pass through the mass center of the telescope. Such an isolation scheme is being used on the Apollo Telescope Mount (ATM), and it is also being considered for some other manned astronomy missions.

1.2 Purpose

It is the purpose of this memorandum to investigate the ATM type gimbal mount and the associated attitude control systems to determine: (1)the pointing accuracy** to be expected from the ATM Pointing Control System (PCS), (2)the significant system parameters so far as telescope pointing accuracy is concerned, and 3)the ultimate pointing accuracy attainable with a gimbal mounted telescope on advanced missions.

1.3 Problem Statement

ATM spacecraft attitude is maintained by means of two interacting feedback control systems, one that controls carrier vehicle attitude and one that points the telescope relative to the carrier. Control Moment Gyroscopes (CMGs)

---

* The resolution of ground based telescopes with apertures of over 12 inches is limited by image smearing resulting from the light passing through the earth's atmosphere.

**The term "pointing accuracy" in this memorandum refers to the accuracy of maintaining a certain telescope attitude, in contrast to the accuracy with which this attitude was initially acquired.

are to be used for ATM carrier attitude control, and CMGs will probably be used on advanced manned astronomy missions as well. Telescope attitude is controlled by torquers located directly on the gimbal axes. In addition to those produced by the torquers, there are torques exerted across the gimbals about the gimbal axes by the gimbal pivots themselves and by cables crossing the interface.

Analysis and computer simulations of the ATM PCS have shown that of all the disturbance forces and torques acting to influence the attitude of the telescope, crew motion disturbances* result in the largest pointing errors. Thus for the ATM, crew motion disturbances are of prime importance in predicting pointing accuracy, and it is expected that this will also be the case for other manned spacecraft with gimbal mounted telescopes.

Crew motions are represented here as time functions possessing the essential features of single astronaut motions; similar representations are being used to design the ATM PCS (see Reference 1). The effects of combined and continuous crew motions are currently being studied by means of a stochastic process crew motion representation, and the results of these studies will be presented later.

At this point it is suggested that the reader review the Conclusions (Page 33), which are organized so as to provide an outline of the intervening material.

2.0 THE EFFECTS OF CERTAIN INDIVIDUAL SOURCES OF ERROR

2.1 The Governing Equations

The telescope pointing accuracy attainable with the PCS depends largely on how successful one is at reducing certain sources of error that exist in the gimbal mounting and the gimbal control system. Provided that one is not doing offset pointing (e.g., observing the sun's limb), the following four sources of error appear to be most important:

Mass Center Offset - This is the distance between the mass center of the telescope and the point at which the gimbal axes intersect.

---

*For a massive spacecraft, it is adequate to represent crew motions as forces and moments exerted on the carrier vehicle rather than as additional bodies moving within the vehicle. Other disturbances are those due to gravitational, aerodynamic, magnetic, and solar pressure phenomena.

Pivot Spring Constant - To virtually eliminate pivot friction, flexure pivots are used in the ATM gimbals. These devices produce a torque about the gimbal axis that is proportional to gimbal rotation angle.

Wire Harness Hysteresis - A cable of approximately 1000 wires crosses the ATM gimbals. The torque vs. rotation characteristic of the harness exhibits hysteresis in addition to a spring constant, which augments the pivot spring constant.

Torquer Nonlinearities - The ATM gimbal torquers possess a so-called threshold or breakout torque, due to magnetic hysteresis.

Equations governing motions of a carrier and a telescope connected by two degree-of-freedom gimbals are derived in Reference 2. In Appendix I of this memorandum these equations are rendered into a form that allows one to comprehend the relation between pointing accuracy and the sources of error listed above. These equations for the spacecraft x-axis (parallel to the long axis of the AAP-3/4 Orbital Assembly)are*

$$[I_1+m(p_2s_2+p_3s_3)]\ddot{\phi}' + K_{rx}\dot{\phi}' + K_{ex}\phi' = M(-F_{1y}s_3 + F_{1z}s_2) + T_{1x} \qquad (2.1)$$

$$[I_2-m(q_2s_2+q_3s_3)]\ddot{\phi} - \tau(i) = -m(p_2q_2+p_3q_3)\ddot{\gamma}_1 + M(F_{1y}q_3-F_{1z}q_2) + T_{g1} \qquad (2.2)$$

where $i = -K_{r1}\dot{\phi} - K_{e1}\phi$

In these equations ϕ' and ϕ are, respectively, the carrier and the telescope x-axis rotation angles, and γ_1 is the gimbal angular displacement about this axis; I_1 and I_2 are the respective carrier and telescope centroidal moments of inertia about the x-axis, and quantities m and M depend on the masses of the two bodies; p_1, p_2, p_3 locate the mass center of the carrier relative to the gimbal center of rotation, q_1, q_2, q_3 specify the mass center offset, and $s_i = p_i - q_i$, $i = 1, 2, 3$; K_{rx}, K_{ex}, K_{r1}, K_{e1} are the control system gains; forces and

---

*See (I-27) and (I-31) in Appendix I.

torques exerted on the carrier due to crew motion have the measure numbers F_{1x}, F_{1y}, F_{1z}, T_{1x}, T_{1y}, T_{1z}; torquer nonlinearities are accounted for by the function $\tau(i)$, which specifies the relationship between commanded and actual torque; lastly, T_{g1} denotes the gimbal pivot torques other than those produced by the torquers. Appendix I gives more complete definitions of the quantities appearing in (2.1), (2.2).

For the z-axis (for the ATM this axis is normal to both the Workshop long axis and the telescope optical axis), equations (I-28) and (I-31) are applicable.

$$[K_1+m(p_1s_1+p_2s_2)]\ddot{\psi}'+K_{rz}\dot{\psi}'+K_{ez}\psi' = M(-F_{1x}s_2+F_{1y}s_1) + T_{1z} \qquad (2.3)$$

$$[K_2-m(q_1s_1+q_2s_2)]\ddot{\psi}-\tau(j) = -m(p_1q_1+p_2q_2)\ddot{\gamma}_2 + M(F_{1x}q_2-F_{1y}q_1)+T_{g2} \qquad (2.4)$$

where $j = -K_{r2}\dot{\psi} - K_{e2}\psi$

Previously undefined quantities are ψ' and ψ, the carrier and telescope z-axis rotation angles; γ_2, the gimbal angular displacement about the z-axis; K_1 and K_2, the respective carrier and telescope centroidal moments of inertia about this axis; and K_{rz}, K_{ez}, K_{r2}, and K_{e2}, the associated control system gains.

2.2 The Torquer Characteristic

It is assumed that the torquers behave ideally except for a so-called breakout torque, which is modeled as coulomb friction.* The resulting characteristics are given by the functions

$$\tau(i) = i - T_{b1} \operatorname{sgn} \dot{\gamma}_1$$

and

$$\tau(j) = j - T_{b2} \operatorname{sgn} \dot{\gamma}_2 \qquad (2.5)$$

*This model was developed after discussions with Mr. Charles Hayes of Inland Motor Corporation, Radford, Va. Inland manufactures the ATM gimbal torquers as well as a line of torquers for other applications.

for the first and second gimbal axes, respectively, where T_{b1} and T_{b2} are the magnitudes of the breakout torques and where

$$\text{sgn } \xi = \xi/|\xi| \quad , \quad \xi \neq 0$$

$$= 0 \quad , \quad \xi = 0$$

Note that (2.5) render (2.2) and (2.4) linear differential equations,* this being advantageous in that the various sources of error may be studied independently.

2.3 System Constants and Crew Disturbances

In order to determine the telescope pointing error attributable to the various sources of error, numerical values must be assigned to the vehicle properties and control system parameters that enter into equations (2.1) - (2.4), and the crew motions must also be defined analytically. Vehicle properties used are those for the current ATM as given on p. A-9 of Appendix I. It is convenient to express the control system gains in terms of the undamped natural frequency and damping ratio of (2.1) - (2.4); thus, we define

$$\omega_x' = \sqrt{\frac{K_{ex}}{I_1+m(p_2s_2+p_3s_3)}} \quad , \quad \omega_z' = \sqrt{\frac{K_{ez}}{K_1+m(p_1s_1+p_2s_2)}}$$

$$\zeta_x' = \frac{1}{2\omega_x'} \frac{K_{rx}}{I_1+m(p_2s_2+p_3s_3)} \quad , \quad \zeta_z' = \frac{1}{2\omega_z'} \frac{K_{rz}}{K_1+m(p_1s_1+p_2s_2)}$$

which apply to the carrier vehicle control system, and

---

*We assume that $|\phi| << |\phi'|$ and consider $\gamma_1 = \phi - \phi'$ to be independent of ϕ, so the term T_{b1} sgn $\dot{\gamma}_1$ is considered as a forcing function rather than a nonlinear term in ϕ; similarly for the relation between γ_2 and ψ.

$$\omega_x = \sqrt{K_{e1}/I_2} \quad , \quad \omega_z = \sqrt{K_{e2}/K_2}$$

$$\zeta_x = \frac{1}{2\omega_x}\frac{K_{r1}}{I_2} \quad , \quad \zeta_z = \frac{1}{2\omega_z}\frac{K_{r2}}{K_2}$$

which apply to the telescope control system. To be consistent with current ATM design philosophy, we assign

$$\omega_x' = \omega_z' = 0.1 \text{ rad/sec} \quad , \quad \zeta_x' = \zeta_z' = 1.0$$

$$\omega_x = \omega_z = 4\pi \text{ rad/sec} \quad , \quad \zeta_x = \zeta_z = 1.0$$

The crew motion disturbances used here are those defined in Appendix II of Reference 2. Results are presented for two disturbances, one representing arm motion of an astronaut located in the LM, and the other representing a wall push-off performed by an astronaut located at the base of the Workshop. These two disturbances appear to be worst-case single crew motions for the AAP Cluster vehicle.

The arm motion crew disturbance is defined in terms of the time function shown in Figure 2.1.

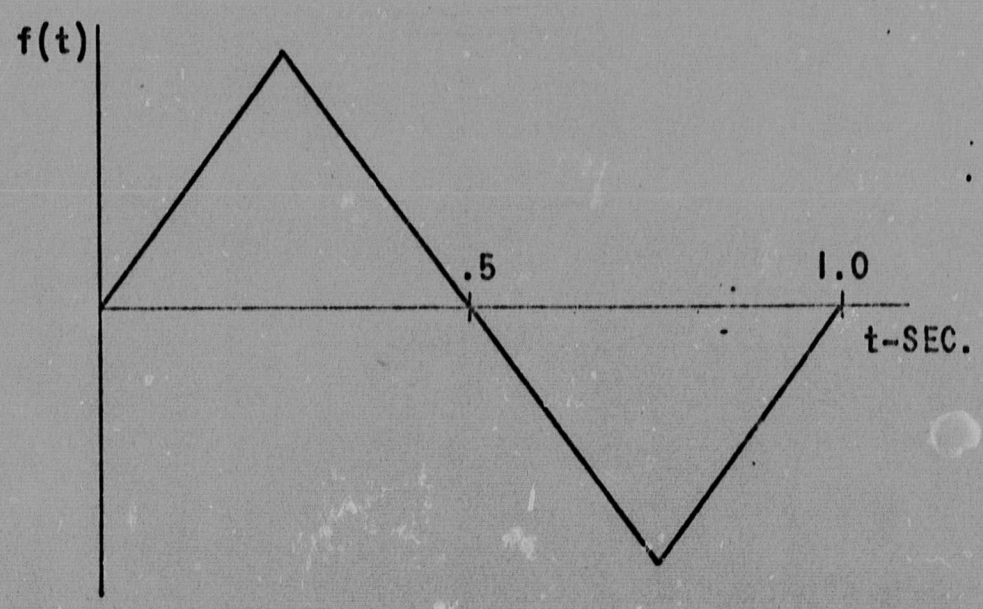

Figure 2.1

Time function representation of arm motion

This function is applied at the LM crew station as a force of 15 lb amplitude to both the x- and z-axes of the vehicle, and it is applied to the y-axis as a moment of 20 ft-lb amplitude. This definition usually results in attitude excursions predominatly about the x-axis.

The wall push-off disturbance is defined in terms of the time function illustrated in Figure 2.2. The function is applied to the vehicle y-axis as a 12 lb amplitude force, and this definition usually results in attitude excursions primarily about the z-axis.

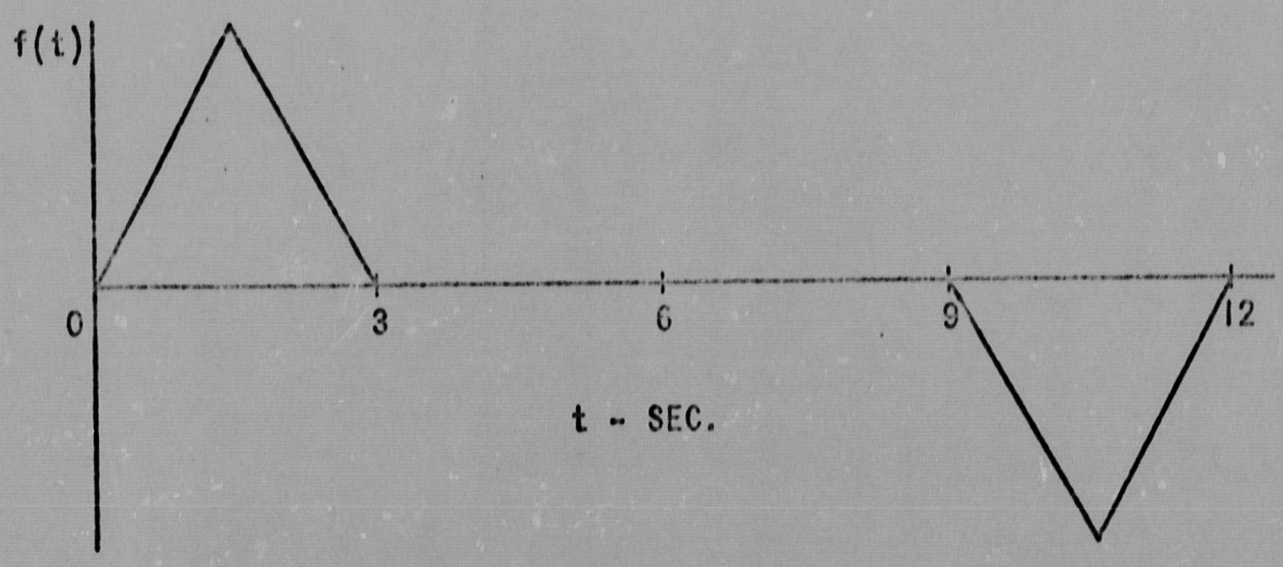

Figure 2.2

Time function representation of a wall push-off

2.4 The Effect of Mass Center Offset

Equations (2.1) and (2.2) and the arm motion crew motion disturbance just defined are used to determine the effect of mass center offset on x-axis telescope pointing accuracy. Numerical calculation shows that the second term in the coefficient of $\ddot{\phi}$ is negligible compared to the first term, I_2, and since $F_{1y}=0$ for the arm motion disturbance and $p_3 << p_2$, it is also apparent that q_2 is a more influential parameter than q_3. If we consider only q_2 as a source of error (2.2) becomes, in view of (2.5),

$$I_2 \ddot{\phi} + K_{r1} \dot{\phi} + K_{e1} \phi = -(mp_2 \ddot{Y}_1 + MF_{1z}) q_2$$

With the assumption that $|\ddot{\phi}| << |\ddot{\phi}'|$ this equation may be written as

$$I_2 \ddot{\phi} + K_{r1} \dot{\phi} + K_{e1} \phi = (mp_2 \ddot{\phi}' - MF_{1z}) q_2$$

and the introduction of

$$\phi_{q2} = \phi / q_2$$

allows us to write

$$I_2 \ddot{\phi}_{q2} + K_{r1} \dot{\phi}_{q2} + K_{e1} \phi_{q2} = mp_2 \ddot{\phi}' - MF_{1z} \qquad (2.6)$$

Results of numerical integration of (2.1) and (2.6) for arm motion in the LM starting at t=0 appear in Figure 2.3. Two curves are presented: in one $\phi_{q2}(t)$ is plotted directly, and the other gives the root mean square value, determined from

$$\phi_{q2rms}(t) = \sqrt{\frac{1}{t} \int_o^t \phi_{q2}^2 (z)\, dz} \qquad (2.7)$$

The latter quantity is usually a more accurate indicator of telescope pointing performance than is $\phi_{q2}(t)$ itself, for the astronomical data gathering process is usually one of integration. As an example, suppose that the telescope has a 0.25 inch mass center offset and that we desire a 2.5 second exposure interval. From Figure 2.3 one can see that a peak pointing error, of .012 arc seconds occurs at t=0.9 seconds, whereas the rms pointing error over the exposure interval is only .005 seconds of arc.

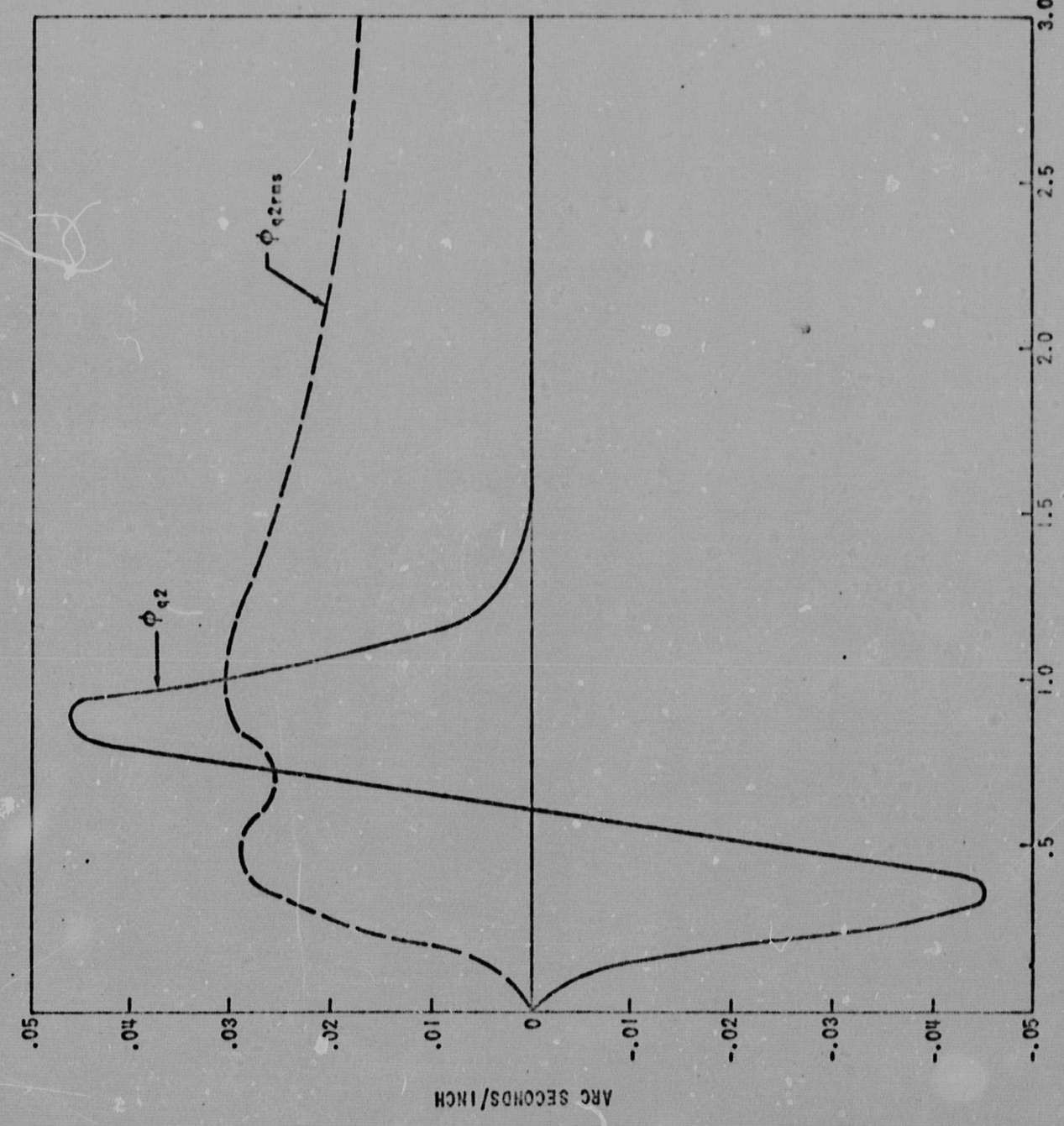

Figure 2.3 The effect of mass center offset a_2 on x-axis pointing accuracy for the arm motion crew disturbance

By proceeding as before, the following equations, analogous to (2.6), are obtained for the z-axis.

$$K_2 \ddot{\psi}_{q1} + K_{r2} \dot{\psi}_{q1} + K_{e2} \psi_{q1} = mp_1 \ddot{\psi}' - MF_{1y} \tag{2.8}$$

$$K_2 \ddot{\psi}_{q2} + K_{r2} \dot{\psi}_{q2} + K_{e2} \psi_{q2} = mp_2 \ddot{\psi}' + MF_{1x} \tag{2.9}$$

Since p_1 and p_2 are of about the same magnitude, there are now two equations for determining the sensitivity of telescope pointing accuracy to the two mass center offsets q_1 and q_2. Figure 2.4 presents results of numerical integrations of (2.3) and (2.8), and Figure 2.5 applies to (2.3) and (2.9); both are based on the wall push-off crew disturbance. One may observe that these two plots are essentially the same, i.e., that pointing accuracy is equally sensitive to mass center offsets in the x direction (q_1) and in the y direction (q_2). Furthermore, for a given mass center offset q_2, the wall push-off crew disturbance (Figure 2.5) results in only about one third the pointing error of the arm motion crew disturbance (Figure 2.3).

2.5 The Effect of Pivot Spring Constant

To investigate this effect for the x-axis equations we let

$$T_{g1} = -K_{g1} \gamma_1$$

where K_{g1} is the spring constant. As before, other sources of error are disregarded, and it is assumed that $|\phi| << |\phi'|$. With the substitution $\phi_{K1} = \phi / K_{g1}$, (2.2) thus becomes

$$I_2 \ddot{\phi}_{K1} + K_{r1} \dot{\phi}_{K1} + K_{e1} \phi_{K1} = \phi' \tag{2.10}$$

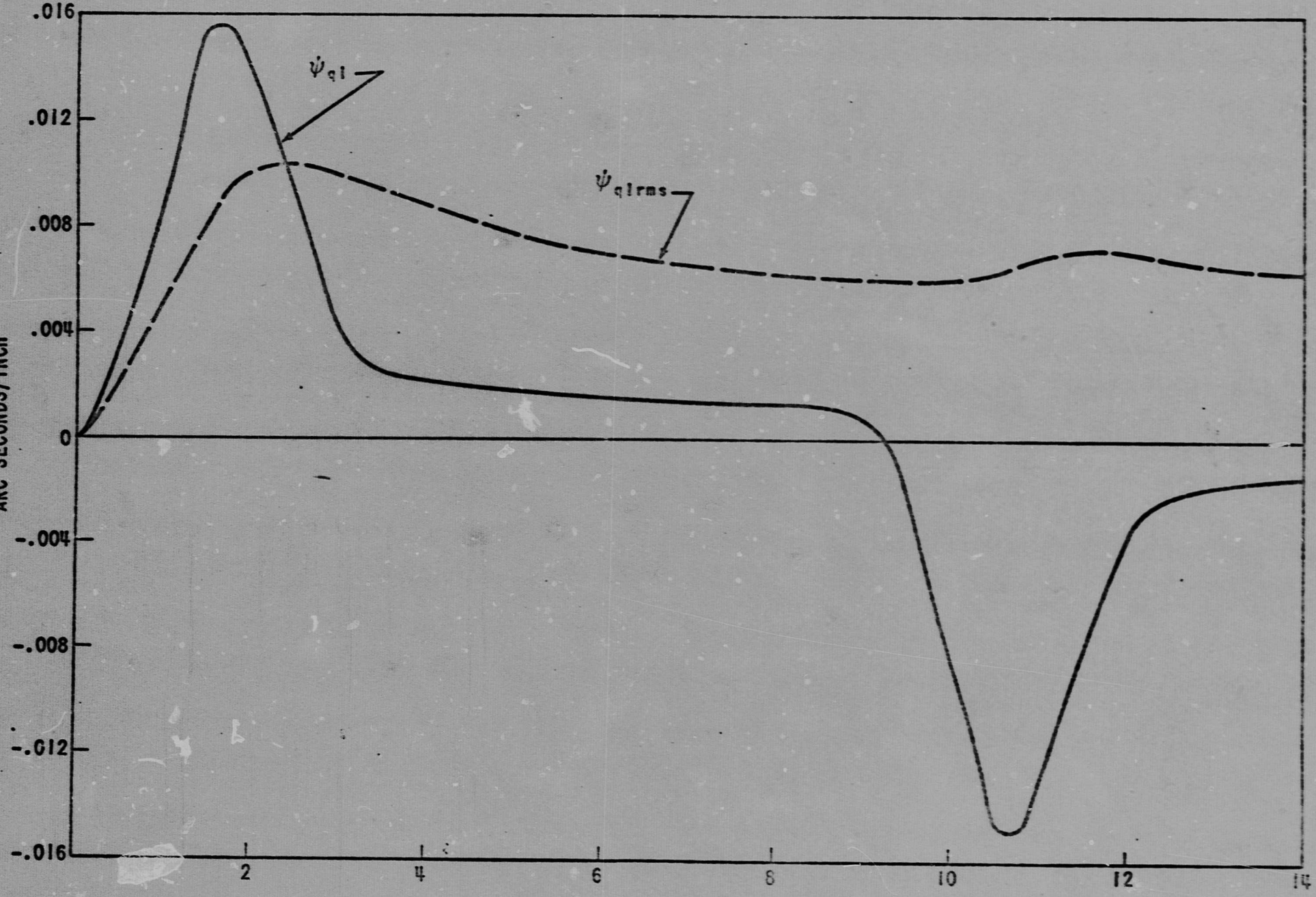

Figure 2.4

The effect of mass center offset q_1 on z-axis pointing accuracy for the wall push-off crew disturbance

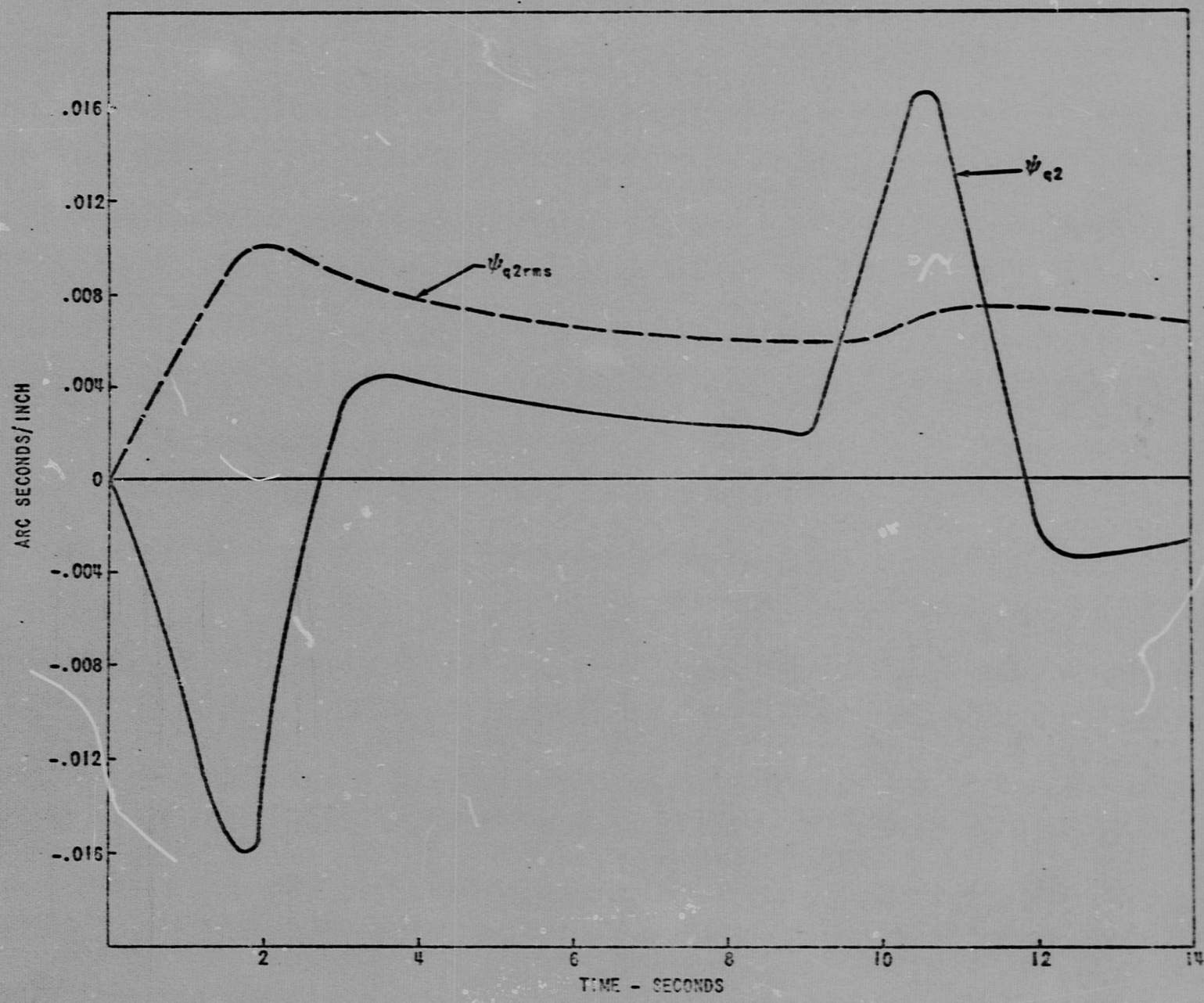

Figure 2.5

The effect of mass center offset q_2 on z-axis pointing accuracy for the wall push-off crew disturbance

Figure 2.6 shows solutions of (2.1) and (2.10) for LM arm motion commencing at t=0. For the ATM, the flexure pivot spring constant is about 4 ft-lb/radian and the wire harness spring constant is about twice this amount (Reference 3); hence, approximately, K_{g1}=12 ft-lb/radian. One may see from Figure 2.6 that this value results in a peak pointing error of only 1.47×10^{-4} seconds of arc, and one may thus conclude that K_{g1} is a relatively insignificant contributor to pointing error.

For motions about the z-axis, an approach similar to the one above leads to

$$K_2 \ddot{\psi}_{K2} + K_{r2} \dot{\psi}_{K2} + K_{e2} \psi_{K2} = \psi' \qquad (2.11)$$

where $\psi_{K2}=\psi/K_{g2}$, K_{g2} being the pivot spring constant about the z-axis. A solution of (2.3) and (2.11) for a wall push-off disturbance is shown in Figure 2.7, from which one obtains a peak pointing error of 3.96×10^{-3} arc seconds when K_{g2}=12 ft-lb/radian. Thus, K_{g2} is a more significant source of error than K_{g1}, but it may be less significant than some of the other sources of error, such as q_2.

2.6 The Effect of Breakout Torque and Wire Harness Hysteresis

Mechanical hysteresis in the wire harness is thought to be due to relative slippage of the wires comprising the harness as it is deformed. This hysteresis is modeled adequately as coulomb friction, just as the torquer breakout torque is, and for the x-axis we have

$$\iota(-K_{r1}\dot{\phi}-K_{e1}\phi) + T_{g1} = (-K_{r1}\dot{\phi}-K_{e1}\phi) - (T_{b1}+T_{h1}) \operatorname{sgn} \dot{\gamma}_1$$

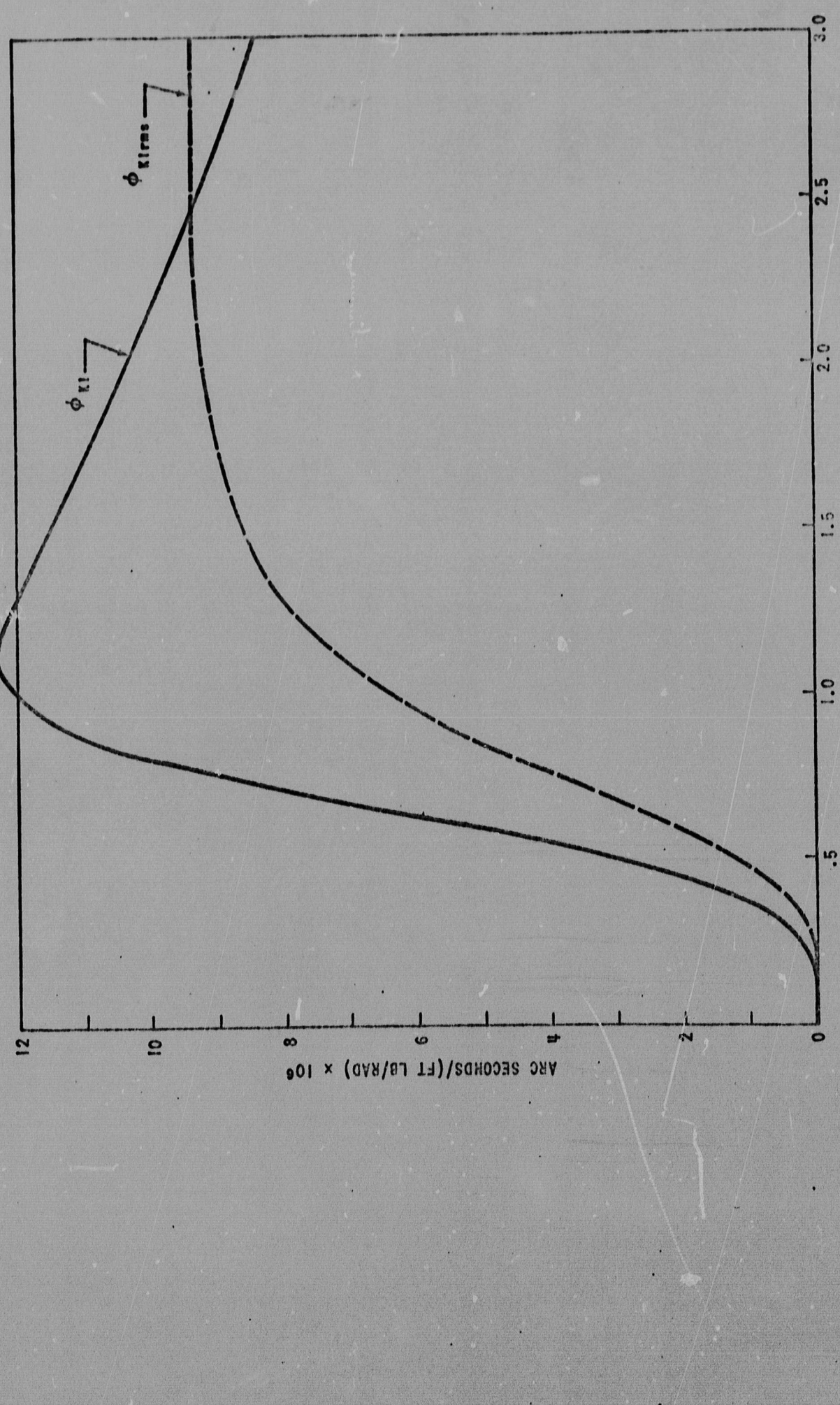

Figure 2.6 The effect of spring constant K_{gl} on x-axis pointing accuracy for the arm motion crew disturbance

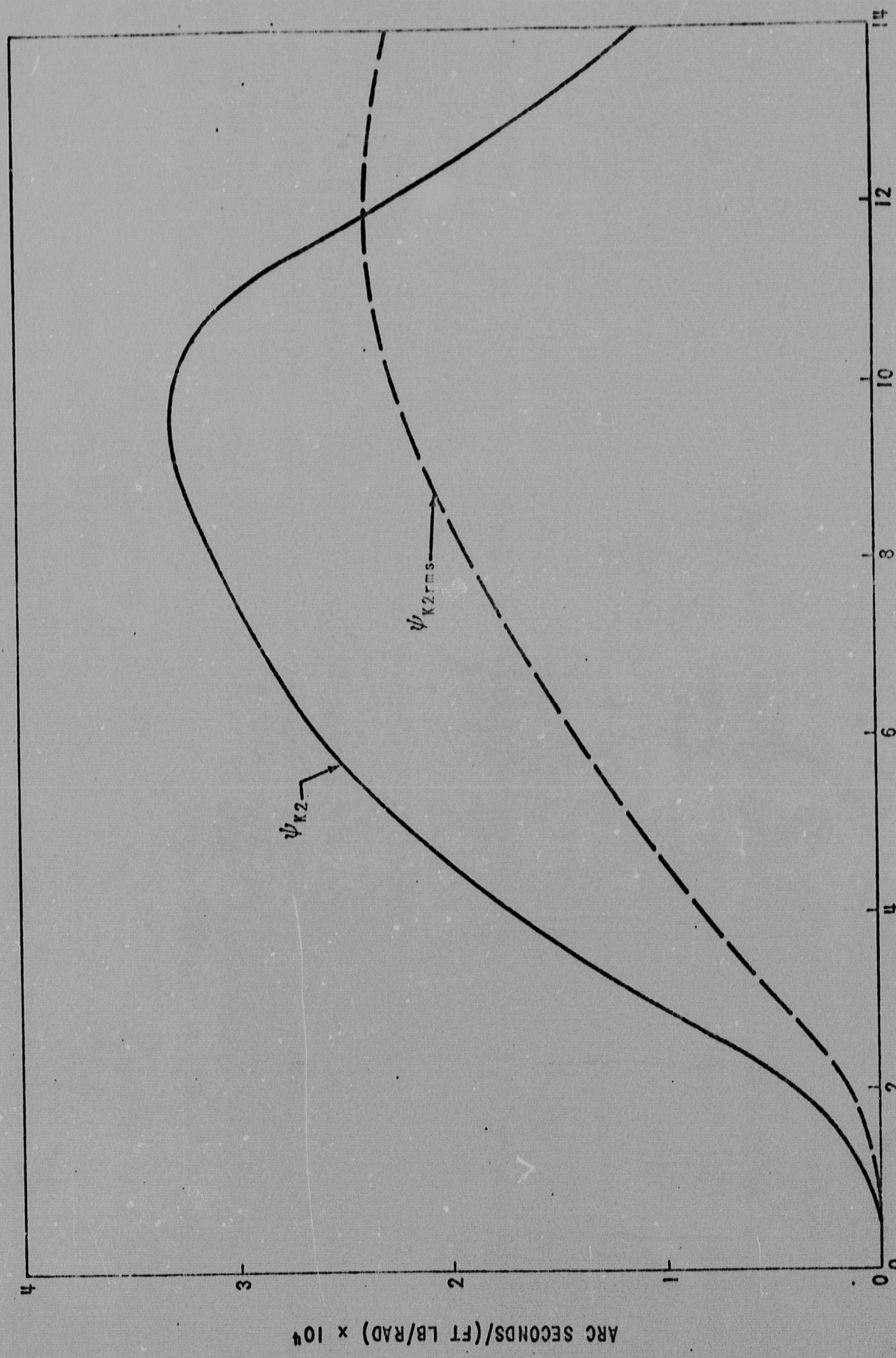

Figure 2.7 The effect of spring constant K_{g2} on z-axis pointing accuracy for the wall push-off crew disturbance

where T_{h1} is the hysteresis torque. It is now assumed that $|\dot{\phi}| << |\dot{\phi}''|$, and only T_{b1} and T_{h1} are considered as sources of error. Equation (2.2) becomes

$$I_2 \ddot{\phi}_{T1} + K_{r1} \dot{\phi}_{T1} + K_{e1} \phi_{T1} = \text{sgn } \dot{\phi}'' \qquad (2.12)$$

where

$$\phi_{T1} = \phi/(T_{b1} + T_{h1}).$$

The essential character of the solutions of (2.12) may be understood by examining the equation itself. It is important to note, for example, that the magnitude of the pointing error attributable to breakout torque and harness hysteresis is determined by the values of K_{e1}, T_{b1}, and T_{h1} rather than by the crew motion disturbance used.

Solutions of (2.1) and (2.12) for arm motion crew disturbances in the LM are presented in Figure 2.8. ATM values of T_{b1} and T_{h1} are approximately .08 ft-lb (Reference 4) and .01 ft-lb (Reference 3), respectively. Thus, it may be seen that for the ATM the pointing error due to these effects is about .05 arc second peak and also .05 arc second rms for exposure intervals of over 0.5 second.

For motion about the z-axis, the equation corresponding to (2.12) is

$$K_2 \ddot{\psi}_{T2} + K_{r2} \dot{\psi}_{T2} + K_{e2} \psi_{T2} = \text{sgn } \dot{\psi}'' \qquad (2.13)$$

in which $\psi_{T2}=\psi/(T_{b2}+T_{h2})$. Figure 2.9 displays a solution of (2.3) and (2.13) for a wall push-off disturbance, and since K_{e2} is almost equal to K_{e1}, one may see that ϕ_{T1} and ψ_{T2} are almost equal in magnitude, as was predicted previously.

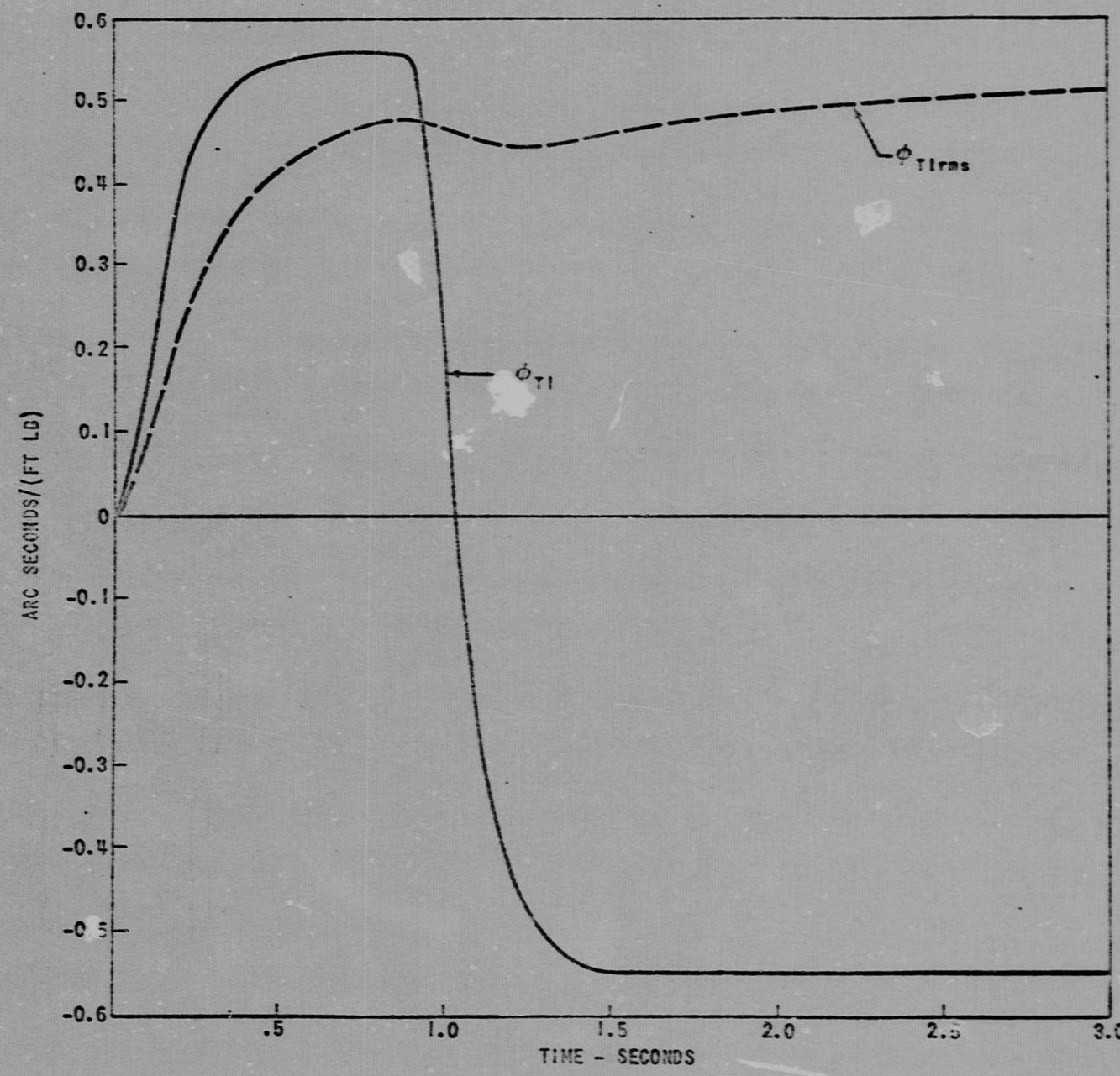

Figure 2.8

The effect of breakout torque and wire harness hysteresis on x-axis pointing error for the arm motion crew disturbance

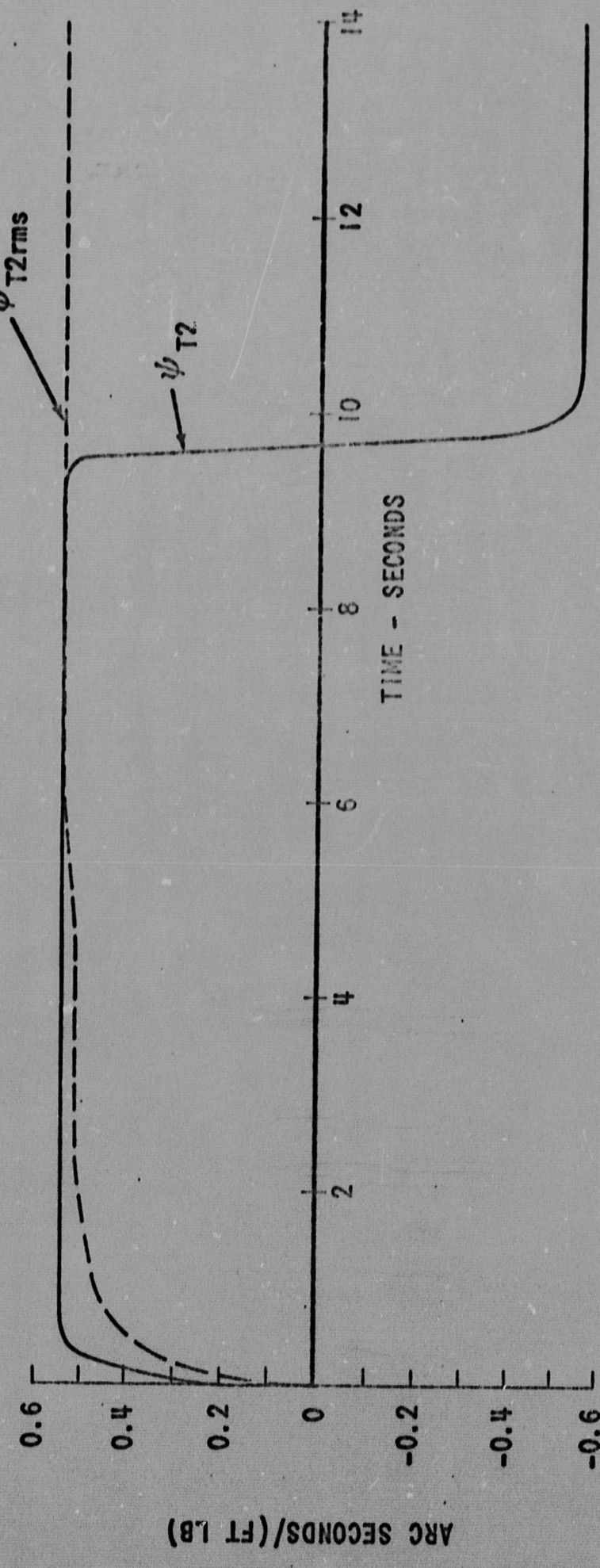

Figure 2.9

The effect of breakout torque and wire harness hysteresis on z-axis pointing error for the wall push-off crew disturbance

3.0 THE EFFECTS OF COMBINED SOURCES OF ERROR

3.1 The Flexible Carrier Model

Although Equations (2.1) - (2.4) lead to useful results so far as individual sources of error are concerned, their validity may be questioned since several assumptions were required to obtain them. In this section the pointing error of a gimbal mounted telescope is investigated by means of a more comprehensive mathematical model, two of whose features are of particular importance:

1. It is a full three dimensional model, as opposed to a single axis one.

2. The carrier vehicle is modeled as a flexible body rather than a rigid one. This is especially important for certain vehicle configurations, such as the AAP Cluster.

This model is not discussed in detail here, since it differs from the one described in Reference 2 only in the following ways:

1. Loads due to aerodynamic and gravity-gradient effects are neglected. These loads are of such low magnitude and frequency in comparison to those exerted by the crew that their effect on telescope pointing accuracy is negligible.

2. The carrier is flexible rather than rigid. This is handled analytically in terms of the mode shapes and frequencies of the carrier vehicle.

3.2 The Modal Data

Modal analyses of the AAP Cluster have been performed by the Martin Marietta Corporation. The analysis reported in Reference 5 is used here to represent the dynamics of the AAP carrier vehicle, and for lack of such information for future vehicles, this analysis is also used to provide typical modal data for an advanced vehicle. So far as the influence of crew motion on telescope pointing accuracy is concerned, computations based on the modal data indicate that the following twenty-five modes are most significant (listed in order of decreasing significance): 1, 2, 3, 4, 5, 6, 8, 7, 16, 17, 12, 28, 27, 24, 11, 15, 10, 14, 25, 31, 44, 18, 26, 13, 42. These twenty-five modes, whose frequencies range from .038 to 2.275 Hz (excluding the rigid body modes), are used in the model, and it is assumed that 1.0 percent of critical damping acts on each mode.

3.3 Comparison of Results for Flexible Carrier and Single Axis Models

The flexible carrier model does have the capability for evaluating all sources of error acting simultaneously. However, before using the model's full potential, it is instructive to evaluate the attitude excursions due to the sources of error acting individually so as to be able to compare results with the simplified model used in Section 2. The following table provides such a comparison. The sources of error are listed in the left column, the types of attitude errors considered are given at the top, and the numbers in the format (flexible body error)/(single axis error) are the attitude excursions in the units given. The sources of error have the numerical values $q_1=q_2=0.25$ in., $K_{g1}=K_{g2}=12$ ft-lb/radian, $T_{b1}+T_{h1}=T_{b2}+T_{h2}=.09$ ft-lb.

Sources of Error	Carrier Peak Error (seconds of arc)	Telescope Peak Error (milliseconds of arc)	Telescope Max RMS Error (milliseconds of arc)	Telescope RMS Error @ t_m * (milliseconds of arc)
Arm Motion				
q_2	6.88/4.65	19.5/11.2	12.7/7.6	12.7/7.6
K_{g1}	6.88/4.65	.22 /.15	.16 /.11	.12 /.08
$T_{b1}+T_{h1}$	6.88/4.65	50.1/50.1	41.9/50.1	38.6/41.8
Wall Push-off				
q_1	124./123.	4.01/3.93	2.69/2.60	1.19/1.74
q_2	124./123.	3.59/4.22	2.12/2.50	1.59/1.76
K_{g2}	124./123.	3.98/3.96	2.85/2.82	2.84/2.82
$T_{b2}+T_{h2}$	124./123.	49.8/49.7	49.8/49.7	47.6/49.7

---

*t_m is the time at the end of the crew motion - 1.0 second for arm motion and 12.0 seconds for the wall push-off.

One sees that the correlation between the models is quite good for the wall push-off crew disturbance, which was in Section 2 associated with motion about the z-axis. For the arm motion crew disturbance, the pointing errors due to q_2 and K_{g1} are 31 to 43 percent lower when the single axis model is used than when the flexible carrier model is used. Most of this difference may be explained as being due to two contributions: First, the pointing error given for the single axis model is only that about the x-axis, whereas the pointing error for the flexible carrier model is the vector sum* of the errors about the x- and z-axes. As the arm motion disturbance actually leads to substantial motions about both axes, one can expect single axis results to be up to 29 percent $(1-1/\sqrt{2})$ lower. The second contribution is due to the particular structural properties of the ATM carrier vehicle. The LM, upon which the arm motion disturbance is exerted and to which the ATM is attached, is connected to the remainder of the carrier by means of a relatively complaint docking structure. Hence, attitude excursions of the telescope mounting are larger than they would be in the case of a rigid docking structure.

3.4 Results for Combined Sources of Error

Based on the following conditions, we present here an analytical prediction of the telescope pointing accuracy obtainable with the current ATM Pointing Control System.

1. Results presented in this section are for observation of the radiometric center of the celestial body being observed. So-called offset pointing is treated independently in Section 4.

2. The prediction is valid only for the single crew disturbances defined previously. These are thought to be, in some sense, worst case single disturbances.

3. Certain phenomena which influence telescope pointing accuracy are not included in this study because it presently seems more satisfactory to consider them independently. These are

---

*Small rotations assumed.

a. Attitude sensor anomalies.* For the ATM the most significant of these is noise in the Fine Sun Sensor, and it causes less than 0.1 arc second rms pointing error.

b. Telescope vibrational distortion.* This effect has been shown to be negligible for the ATM, provided that one uses control system gains no larger than those given in Section 2.3 (Reference 6).

c. Telescope thermal distortion. Although this problem has been excluded from this study, it may well limit the pointing accuracy attainable with the ATM as well as other orbiting telescopes, especially solar telescopes.

In addition to the conditions just stated, results presented in this section are based on the numerical values used earlier in this work for the sources of error,

$q_1 = q_3 = 0.25$ inch, $q_2 = -0.25$ inch**

$K_{g1} = K_{g2} = 12$ ft-lb/radian

$T_{b1} + T_{h1} = T_{b2} + T_{h2} = .09$ ft-lb

Figure 3.1 presents the predicted attitude behavior for astronaut arm motion in the LM starting at t=0, and Figure 3.2 presents the same information for a wall push-off at the base of the Orbital Workshop. The curves have the same interpretation as those in Section 2, except that the pointing error is no longer due to just a single source of error, and pointing error no longer represents rotations about just a single axis. In addition to the curves, each figure gives numerical values for four parameters of the motion, the definitions and significance of which are now given.

---

* These items are currently being studied at Bellcomm in connection with a gimbal mounted one meter stellar telescope.

**A negative sign is assigned to q_2 so that the sources of error q_1, q_2, and K_{g2} will make the largest possible total contribution to pointing error; cf. Figures 2.5, 2.6, and 2.8.

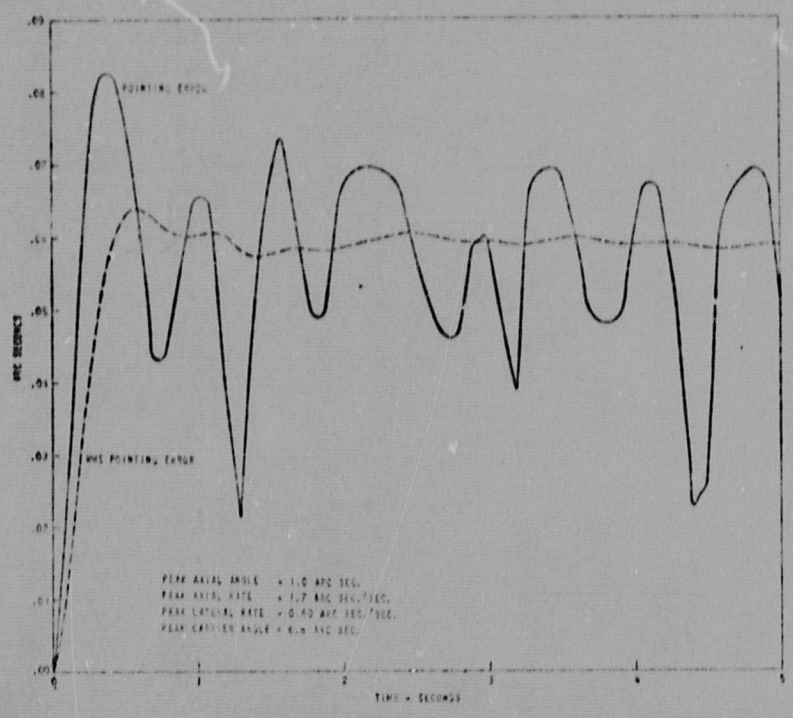

Figure 3.1

Predicted telescope response to arm motion

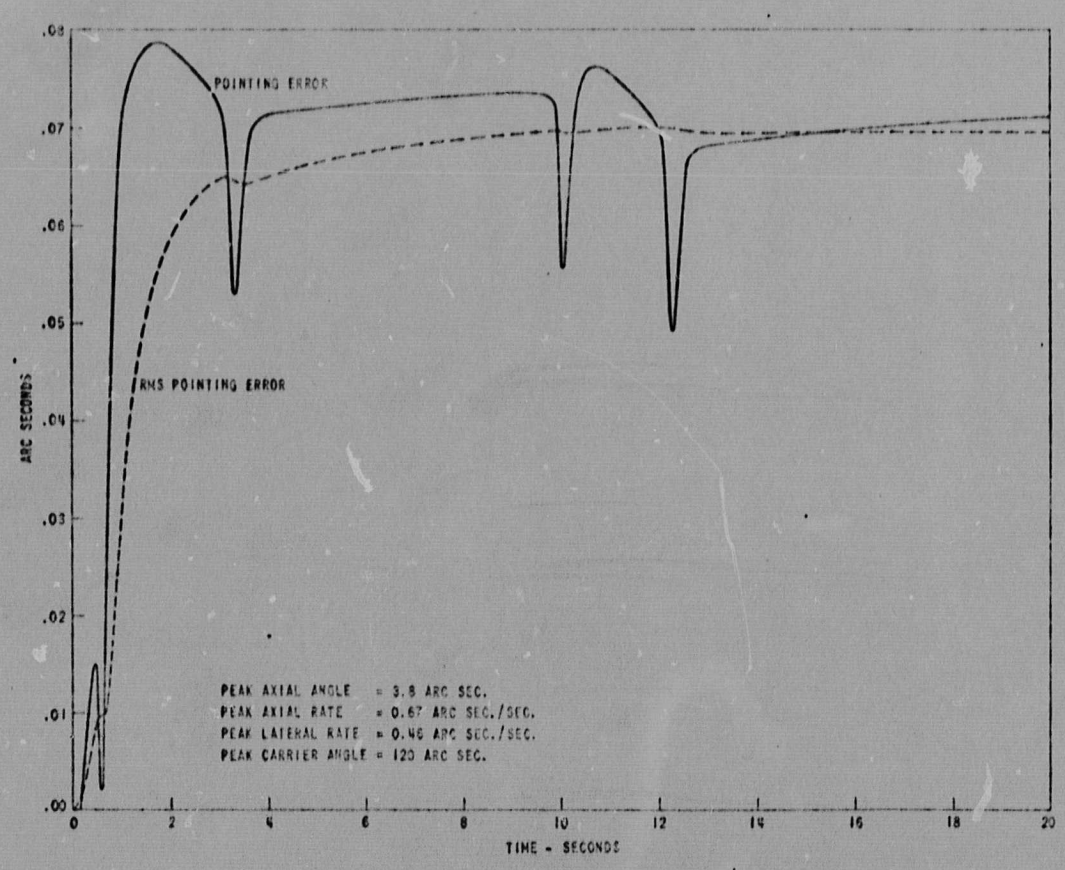

Figure 3.2

Predicted telescope response to a wall push-off

Peak lateral rate - If the telescope angular velocity is resolved into components parallel to and normal to the line of sight, we define the maximum magnitude of the latter component to be the peak lateral rate.* This parameter is of importance for instruments requiring small excursions for only a very short time interval, an example of which would be the photoheliograph, sometimes called the Zirin telescope, currently being developed at the Jet Propulsion Laboratory for an advanced ATM. A typical exposure interval for this instrument is 25 milliseconds, and one can thus see, by reference to the peak lateral rate given in Figure 3.1, that the telescope will move no more than .015 second of arc during such an exposure.

Peak axial angle - This refers to the maximum angular excursion of the telescope (and the carreir) about the line of sight. It gives an indication of image motion at the periphery of a large field of view.

Peak axial rate - Simply the time derivative of the above quantity.

Peak carrier angle - This is the maximum attitude excursion of the carrier at the telescope attach point about any axis normal to the line of sight. If the telescope mounting gimbals are caged (locked), this quantity is also the peak telescope pointing error. Peak carrier angle then, in combination with the peak pointing error (uncaged), provides a figure of merit for the gimbal mounting, for it shows how effective the gimbals are in removing carrier attitude excursions.

Figures 3.3 and 3.4 exhibit the pointing behavior for arm motion and wall push-off, respectively, under the assumption that the carrier vehicle is rigid. Comparison of Figures 3.1 and 3.3 shows that the telescope pointing error is quite similar for the flexible and the rigid vehicles, except that carrier motion and telescope pointing error at the beginning of the crew motion ($t<0.25$ second) are larger

---

*Note that the maximum value of the time derivative of pointing error provides a lower bound on the peak lateral rate; for if the pointing error is denoted ε, $\varepsilon = \sqrt{\phi^2 + \psi^2}$, and $\dot{\varepsilon} = (\phi\dot{\phi} + \psi\dot{\psi})/\varepsilon \leq \sqrt{\dot{\phi}^2 + \dot{\psi}^2}$, as may be demonstrated.

for the flexible vehicle.* In comparing Figures 3.2 and 3.4 one finds the two cases even more similar, except that now the telescope pointing error at the outset (t<1.0 second) is smaller for the flexible carrier. The difference between the results for arm motion (Figures 3.1 and 3.3) and wall push-offs (Figures 3.2 and 3.4) for small t may be explained with the type of argument introduced at the end of Section 3.3. That is, if the docking structure is relatively complaint, as is the case for the ATM carrier vehicle, then crew motions on the ATM side of the docking structure, e.g., LM arm motion, would usually result in larger displacements on the ATM side of the docking structure than would be experienced by a rigid carrier, whereas the docking structure compliance would usually provide some isolation from disturbances not on the ATM side of the compliant structure, e.g., wall push-offs.

As one may see by comparing Figures 3.1 and 3.2, the telescope pointing error appears to be relatively independent of the magnitude of the carrier excursions. This being the case, Figures 3.5 and 3.6 are presented to show the pointing behavior for arm motion and a wall push-off, respectively, when certain parameters associated with carrier motion are assigned particularly conservative values. The changes from the basic case (Figures 3.1 and 3.2) are these:

1. The CMG feedback gains, which have heretofore had the values assigned in Section 2.3, are set to zero. The CMGs are primarily intended to cope with low magnitude, low frequency torques, such as those due to gravity, rather than the torques resulting from crew motion. Since the CMGs are in fact ineffective in responding to crew motion, and since there is some disagreement as to how completely the CMGs need be modeled, we propose to determine telescope pointing accuracy with no CMGs.

2. All twenty-five modes listed in Section 3.2 are used to determine the carrier motion; previously; only the first twenty modes listed had been used. The accuracy of these additional modes is questionable, but they do involve frequencies higher than those previously used.

---

*The flexible vehicle could show a substantial increase in pointing error when acted upon by continuous crew disturbances, due to lightly damped carrier resonances.

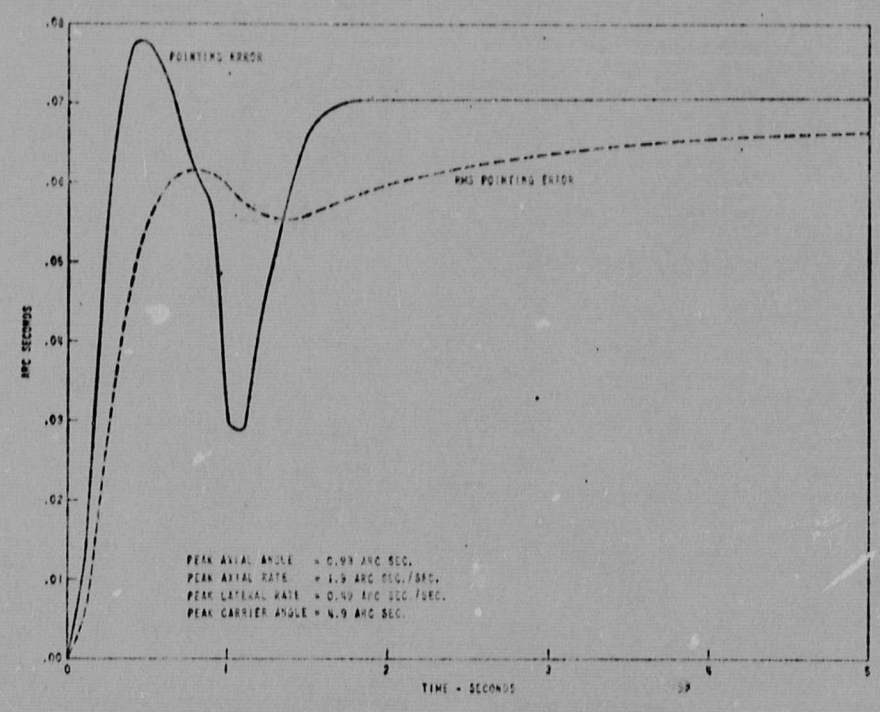

Figure 3.3

Response to arm motion for a rigid carrier

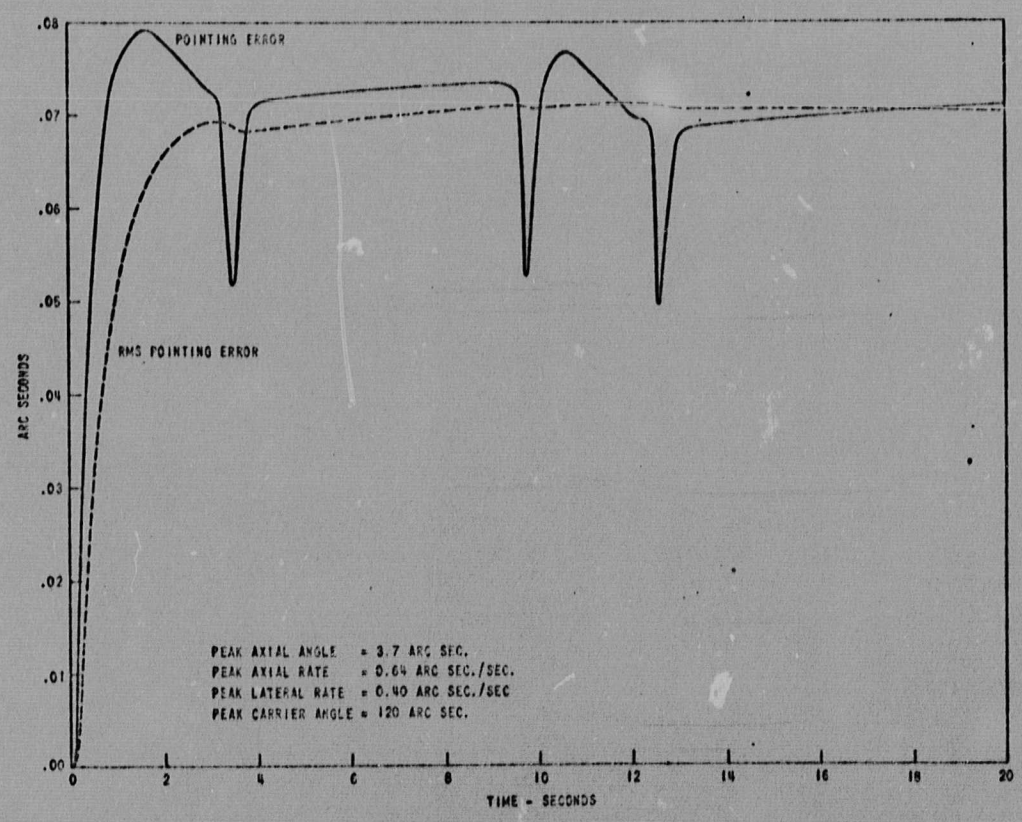

Figure 3.4

Response to a wall push-off for a rigid carrier

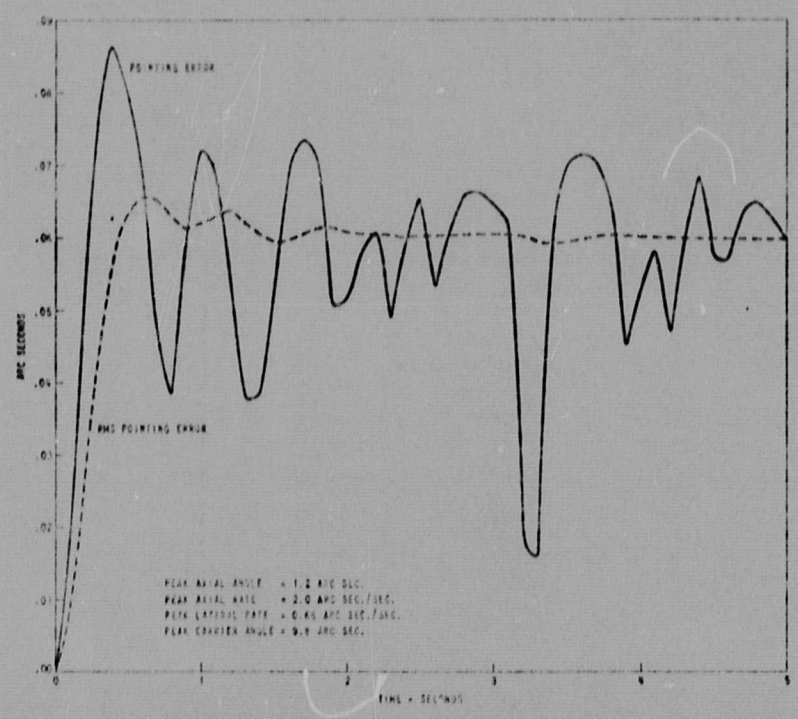

Figure 3.5

Response to arm motion for conservative values of parameters

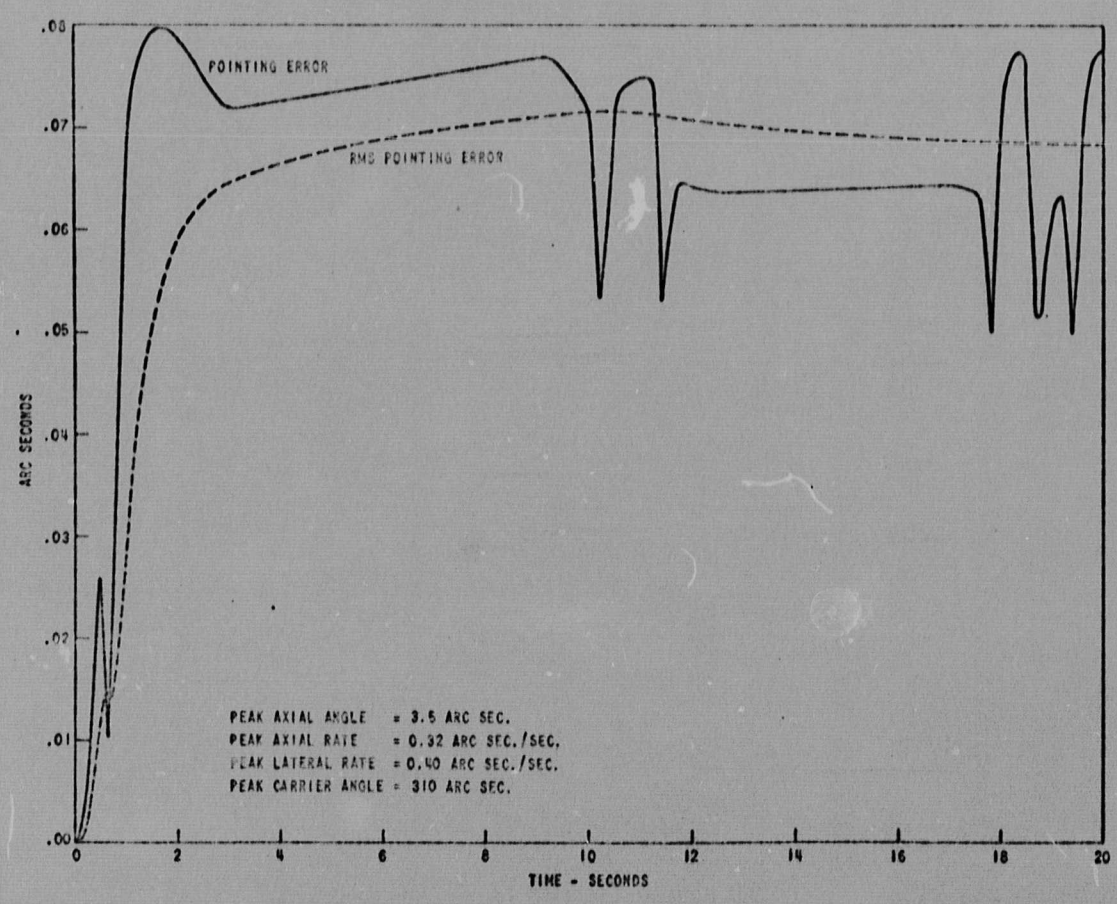

Figure 3.6

Response to a wall push-off for conservative values of parameters

3. Structural damping for all carrier modes is set to zero. Since our crew motions are not repetative, the amount of damping should be unimportant. However, this provides a set of worst case numbers for quantities whose exact values are unknown.

Comparison of Figures 3.1 and 3.5 shows that the telescope pointing error is generally about 10 percent higher for the more conservative set of parameters, although the latter yields about 70 percent higher peak carrier angle than given in Figure 3.1. The insensitivity of telescope pointing error to changes in parameters that affect carrier motion is even more dramatic when the wall push-off is considered: the more conservative parameters generally give less than a 10 percent increase in pointing error and they actually yield a decrease in peak lateral rate (compared to Figure 3.2), despite the fact that the peak carrier angle is 2.5 times greater in Figure 3.6 than in Figure 3.2.

3.5 Pointing Performance of a More Advanced Gimbal Mounting than the ATM

An analytical prediction of the pointing capability of the current ATM was given in the last section. From that discussion it should be clear that the most promising route for obtaining even more accurate pointing is by reducing the sources of error within the telescope gimbal mounting, rather than by trying to reduce the carrier vehicle excurisions, i.e., rather than by use of improved CMGs or better structural design, for example. Using this approach, we show here how the pointing error of the ATM could be reduced to the vicinity of .01 seconds of arc. A set of numberical values for the sources of error that will meet this objective is now given, along with a discussion of how the sources of error might be reduced to these values.

Mass center offset $q_1=q_3=.05$ in, $q_2=-.05$ in. This implies for the ATM an unbalance of 270 in-lb about each axis. The experiment package can be balanced to within this tolerance before launch (Reference 7), although balancing in orbit is also possible. The difficulty with balancing in orbit lies in measuring unbalance in free fall ("zero -g"), but schemes have been devised for doing this.*

---

*See Reference 8 for a description of such schemes.

Pivot spring constant $K_{g1}=K_{g2}=5$ ft-lb/radian. Flexure pivots with adjustable spring constants have recently been incorporated into the ATM design. These can be adjusted to as small a constant as desired, or perhaps even a negative value to partially compensate for the spring constant of the wire harness.

Breakout and wire hysteresis torques $T_{b1}+T_{h1}=T_{b2}+T_{h2}=$ .01 ft-lb. As discussed in Appendix II, there are several means available for modifying the ATM gimbal torquers so as to achieve an order-of-magnitude reduction in T_{b1} and T_{b2}. Wire harness hysteresis could be eliminated by removing the wire harness and handling the transfer of power and data by some other means, such as a chain link transfomer (Reference 9). Also, one might be able to build or route the harness so as to reduce breakout torque, possibly at the expense of pivot spring constant; the increased spring constant could then be compensated, as explained above.

Figures 3.7 and 3.8 portray the pointing behavior for the sources of error just specified due to the arm motion and wall push-off disturbances, respectively. These figures, which are respectively comparable to Figures 3.1 and 3.2 for the standard values of the sources of error, exhibit a peak pointing error of approximately .01 seconds of arc for both crew motions.

4.0 THE POINTING ERROR ASSOCIATED WITH OFFSET POINTING

4.1 Introduction

It has been tacitly assumed in the foregoing that the two gimbal axes are initially perpendicular to the telescope line of sight. This condition ensures that any motion of the carrier about an axis normal to the line of sight can be removed by rotations of the two gimbals. However, because of inevitable small misalignments, the line of sight is not precisely normal to the gimbal axes, and moreover, one may wish to do offset pointing, which also violates the perpendicularity condition. In offset pointing, one biases, either electrically or optically, the telescope attitude sensor signal so as to move the line of sight away from the line to the radiometric center of the object being observed, and thus the line of sight is no longer normal to the gimbal axes.

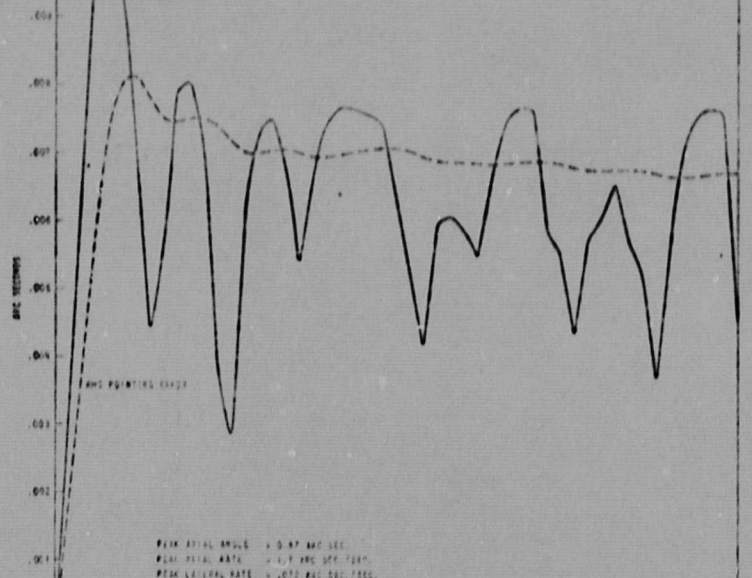

Figure 3.7

Response to arm motion for reduced values of the sources of error

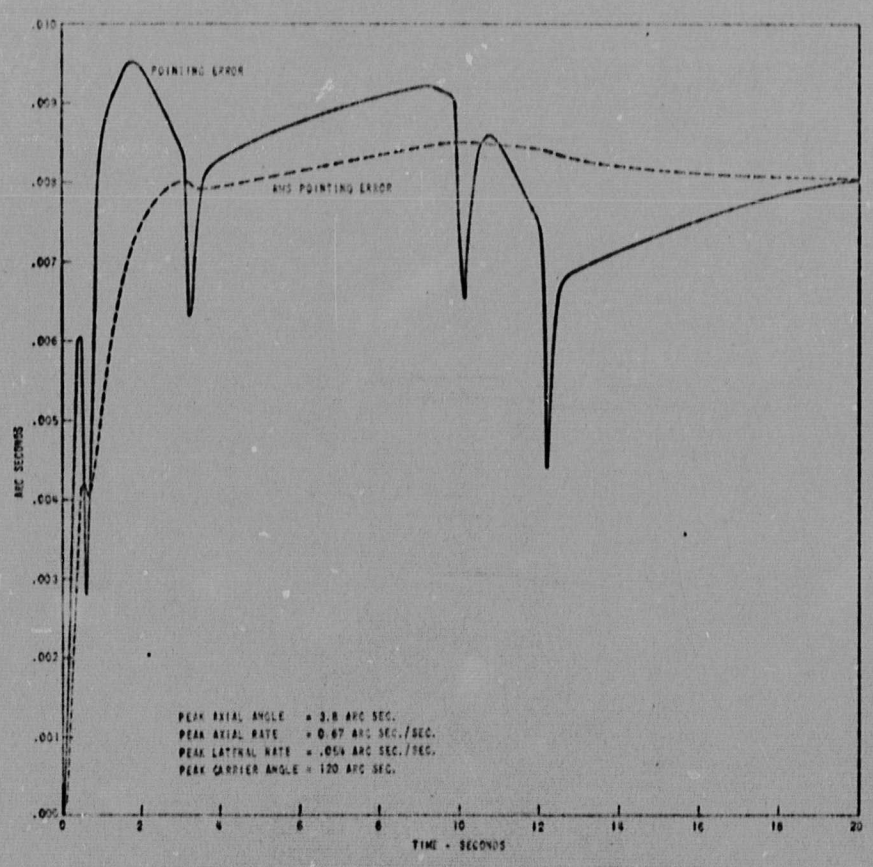

Figure 3.8

Response to a wall push-off for reduced values of the sources of error

Offset pointing is used in the ATM to make detailed observations of any selected point on the solar disc, the diameter of which is approximately 32 minutes of arc. In this section we determine the telescope pointing error associated with making observations of the edge of the solar disc.

4.2 Definition of Pointing Error

The telescope pointing error, denoted by E, depends on the telescope rotation about the x-axis, denoted by ϕ, and the rotation about the z-axis, denoted by ψ:

$$E = \sqrt{\phi^2 + \psi^2} \tag{4.1}$$

So long as all of the angles involved remain small enough, ϕ and ψ may be determined sufficiently accurately from†

$$\phi = \phi' + \gamma_1 \quad , \quad \psi = \psi' + \gamma_2 \tag{4.2}$$

To study offset pointing we require equivalent expressions which allow for sufficiently large values of γ_1 and γ_2; such expressions, derived in Appendix III, are

$$\phi = \frac{1}{2}[\phi'(\cos\gamma_2+\cos\gamma_2^*)\cos(\gamma_1-\gamma_1^*) + \theta'(\cos\gamma_1^*\sin\gamma_2+\sin\gamma_2^*\cos\gamma_1) + \psi'(\sin\gamma_1^*\sin\gamma_2+\sin\gamma_2^*\sin\gamma_1) + (\cos\gamma_2+\cos\gamma_2^*)\sin(\gamma_1-\gamma_1^*)] \tag{4.3}$$

$$\psi = \frac{1}{2}\{-\phi'\sin(\gamma_1-\gamma_1^*)\sin(\gamma_2-\gamma_2^*) - \theta'(\sin\gamma_1+\sin\gamma_1^*)\cos(\gamma_2-\gamma_2^*) + \psi'(\cos\gamma_1+\cos\gamma_1^*)\cos(\gamma_2-\gamma_2^*) + [1+\cos(\gamma_1-\gamma_1^*)]\sin(\gamma_2-\gamma_2^*)\} \tag{4.4}$$

---

†The symbols ϕ', γ_1, ψ', and γ_2 are defined in Section 2.1.

Here θ' is the angular rotation of the carrier about the y-axis, i.e., about the telescope line of sight when $\gamma_1=\gamma_2=0$; and γ_1^* and γ_2^* are the desired values of the gimbal angles (as opposed to the actual values γ_1 and γ_2). Angles ϕ and ψ are rotations about the telescope x- and z-axes, respectively, and they are defined such that $\phi=0$, $\psi=0$ whenever $\phi'=\theta'=\psi'=0, \gamma_1=\gamma_1^*, \gamma_2=\gamma_2^*$.

4.3 Results

Crew motions that result in large angular excursions about the y-axis are of interest when doing offset pointing. This type of motion can be arranged by redefining the wall push-off so that the force is applied parallel to the z-axis, rather than parallel to the y-axis, as done previously.

Figure 4.1 shows the telescope pointing error for this crew motion disturbance and for the gimbal angles $\gamma_1^*=\gamma_2^*=$ 680 arc seconds, values that correspond to observation of the

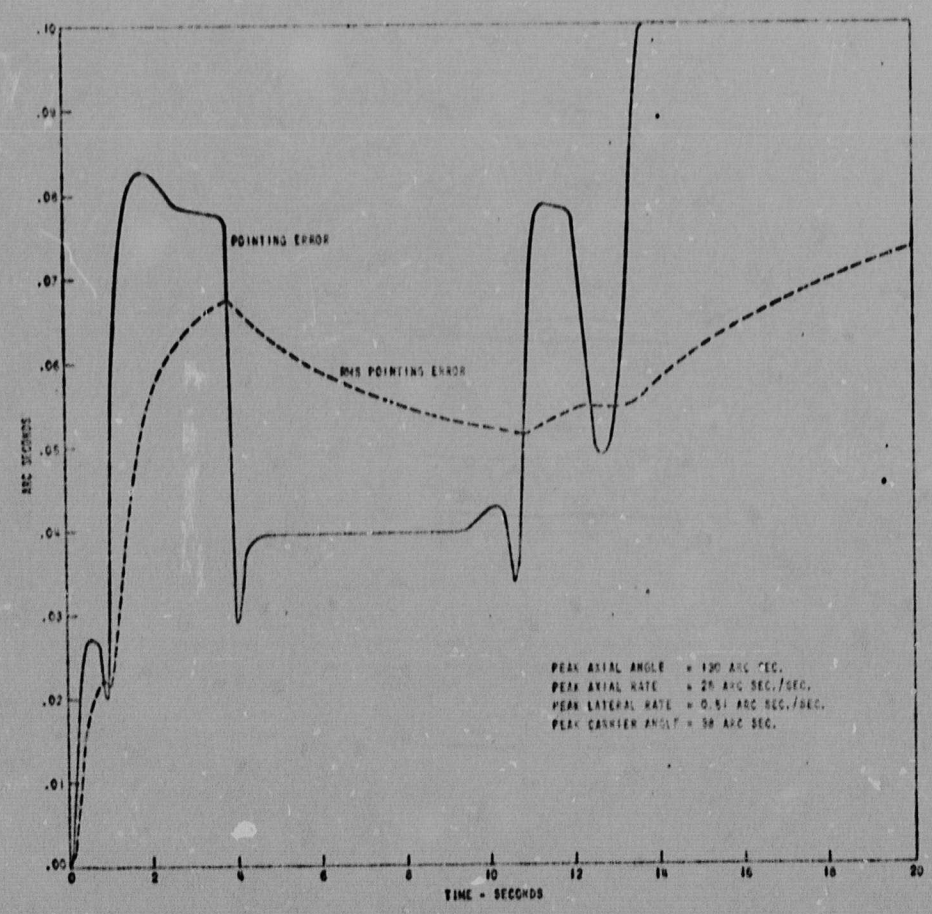

Figure 4.1

Telescope pointing error when viewing the sun's limb

sun's limb. Part of the difference between this plot and some of the preceding ones, e.g., Figure 3.2, is apparently due to the constant torques $K_{g1}\gamma_1^*$ and $K_{g2}\gamma_2^*$ existing about the gimbal axes by virtue of the relatively large values of γ_1^* and γ_2^*. Figure 4.2, which is obtained by setting $K_{g1}=K_{g2}=0$, demonstrates the significance of the pivot spring torques. In order to determine the influence of offset pointing on pointing accuracy in the absence of pivot spring torques, Figure 4.3, for which $\gamma_1^*=\gamma_2^*=0$, is provided. Comparison of this figure with Figure 4.2 shows that, indeed, the pointing error attributable to offset pointing is mostly due to the constant torques $K_{g1}\gamma_1^*$ and $K_{g2}\gamma_2^*$.

The effect of $K_{g1}\gamma_1^*$ and $K_{g2}\gamma_2^*$ on the telescope attitude warrants further examination. By substituting equations (2.5) into (2.2) and (2.4), respectively, and by replacing the gimbal torques T_{g1} in (2.2) and T_{g2} in (2.4) by the constants $K_{g1}\gamma_1^*$ and $K_{g2}\gamma_2^*$, respectively, it may be seen that the telescope attitude response is

$$\phi = K_{g1}\gamma_1^*/K_{e1}$$

$$\psi = K_{g2}\gamma_2^*/K_{e2}$$

That is, $K_{g1}\gamma_1^*$ and $K_{g2}\gamma_2^*$ result in <u>constant</u> attitude displacements of the telescope. Now according to the definition of pointing accuracy given in a footnote in Section 1.1, these constant displacements may be assigned to the catagory of acquisition error rather than pointing error, and it may be said that the pointing error due to an offset of a quarter of a degree is negligible in comparison with that due to other sources of error, even when the spring constants K_{g1} and K_{g2} are considered.

5.0 CONCLUSIONS

Sets of linear, constant coefficient differential equations are presented in Section 2 for each of the two gimbal axes. These equations are solved to give the approximate pointing error, but more importantly, they provide one with insight into the nature of pointing error and of its dependence on the sources of error. For example, one sees that to a first approximation the effects of sources of error may be added.

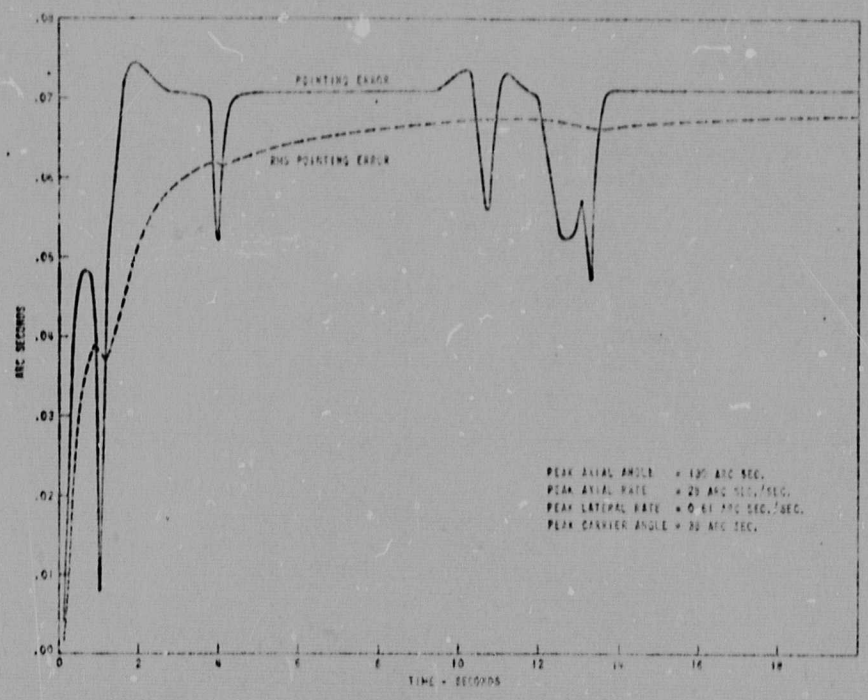

Figure 4.2

Pointing error when viewing the sun's limb for $K_{g1}=K_{g2}=0$

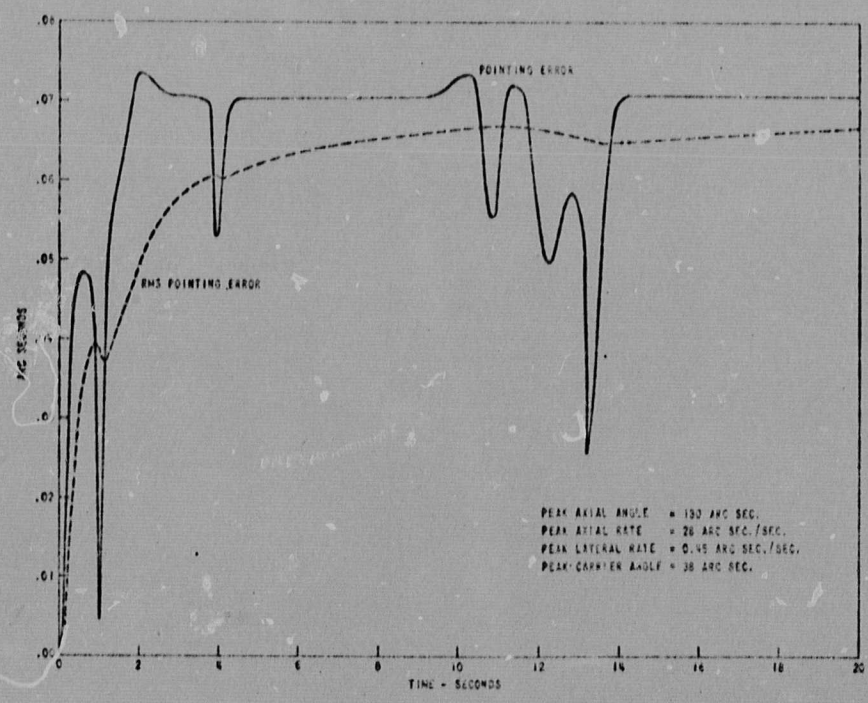

Figure 4.3

Pointing error when viewing the center of the solar disc for for $K_{g1}=K_{g2}=0$

Numerical results are presented in Figures 2.3 - 2.9 in the form of sensitivities of the pointing error to each source of error. The information presented in these figures may be summarized as follows: the sensitivity of telescope pointing error to mass center offset is less than .05 arc second per inch of offset; the sensitivity to pivot spring rate is at most .0004 arc second per ft-lb/radian; and the sensitivity to wire harness hysteresis or breakout torque is less than 0.6 arc second per ft-lb. Although these numbers apply specifically to the ATM configuration, they provide a guide for other types of spacecraft as well; and it should be stressed that under certain circumstances, e.g., short exposure intervals the sensitivities can be much lower than those given.

Section 3 presents results obtained from a more elaborate, three dimensional, flexible body model. The table given in Section 3.3 shows clearly that for the ATM, torquer breakout torque is a larger contributor to pointing error than mass center offset, pivot spring rate, or wire harness hysteresis. Results presented in Figures 3.1-3.6 show that the pointing error of the current ATM design should be less than 0.1 seconds of arc. However, this number does not include the error due to sensor anomalies or thermal distortion, either of which could be significant; it seems more satisfactory to study these phenomena separately, inasmuch as they are not problems unique to the gimbal mounting or even to manned spacecraft. Figures 3.3 and 3.4 indicate that the ATM carrier vehicle flexibility does not have a significant influence on telescope pointing accuracy; moreover, Figures 3.5 and 3.6 show that certain other parameters having to do with carrier vehicle motion have little effect on telescope pointing error, even though their effect on carrier motion is large.

In Section 3.5 is presented a set of reduced values for the sources of error which, if achievable, would reduce the ATM pointing error to the vicinity of .01 seconds of arc. These values indicate the magnitudes of the sources of error that can be tolerated consistent with .01 arc second pointing accuracy. There seems to be little doubt that such values, or even smaller values, are in fact achievable. The encouraging results just given do not imply that the most satisfactory means of achieving .01 arc second pointing is by reducing the sources of error in the ATM: at least two other approaches warrant consideration. One is an entirely different isolation scheme, such as suspension of the telescope by electromagnetic devices; the other retains the gimbals but incorporates more sophisticated control functions that could reduce pointing error without requiring reductions in the values of the sources of error.

The subject of offset pointing is treated in Section 4, where it is shown that the ATM pointing error is essentially the same for observation of the edge of the solar disc as it is for observation of the center of the disc. A significant difference between the two types of observations is that offset pointing results in a constant telescope attitude error due to the pivot spring being displaced through the relatively large gimbal angle. However, this constant attitude error does not affect the data gathering process, and hence, it is more accurately referred to as an acquisition error rather than a pointing error. It should be noted that certain angular misalignments in the sensors and the gimbals result in a condition equivalent to offset pointing, i.e., a condition in which the gimbal axes are not perpendicular to the line of sight. Our statement about the insensitivity of pointing accuracy to gimbal offset can thus be extended to include insensitivity to these angular misalignments, provided that the latter are less than the sun's apparent angular radius (about 16 arc minutes).

ACKNOWLEDGEMENT

The author wishes to express his appreciation to Miss Carol Banick and Mrs. Barbara Lab, who developed the computer programs used in this work.

P. G. Smith

1022-PGS-mef

Attachments
Appendicies I, II, III
References

APPENDIX I

Derivation of Simplified Equations of Motion

Reference 2 presents a set of differential equations representing the attitude and control dynamics of the system described in Section 1.3. In this appendix these equations are rendered into tractable form by making certain assumptions about their behavior. Some of these assumptions are clearly justifiable and others are less so. It is therefore necessary to check the results obtained from the simplified equations against numerical solutions of the complete equations in order to verify the validity of the assumptions.

Problem Statement

Consider two rigid bodies, a carrier B_1 and a telescope B_2, that are connected by means of a set of rigid, massless, two degree-of-freedom gimbals. As shown in Figure I, the sets of mutually perpendicular axes $x_i y_i z_i$, i=1,2, are fixed in B_i.

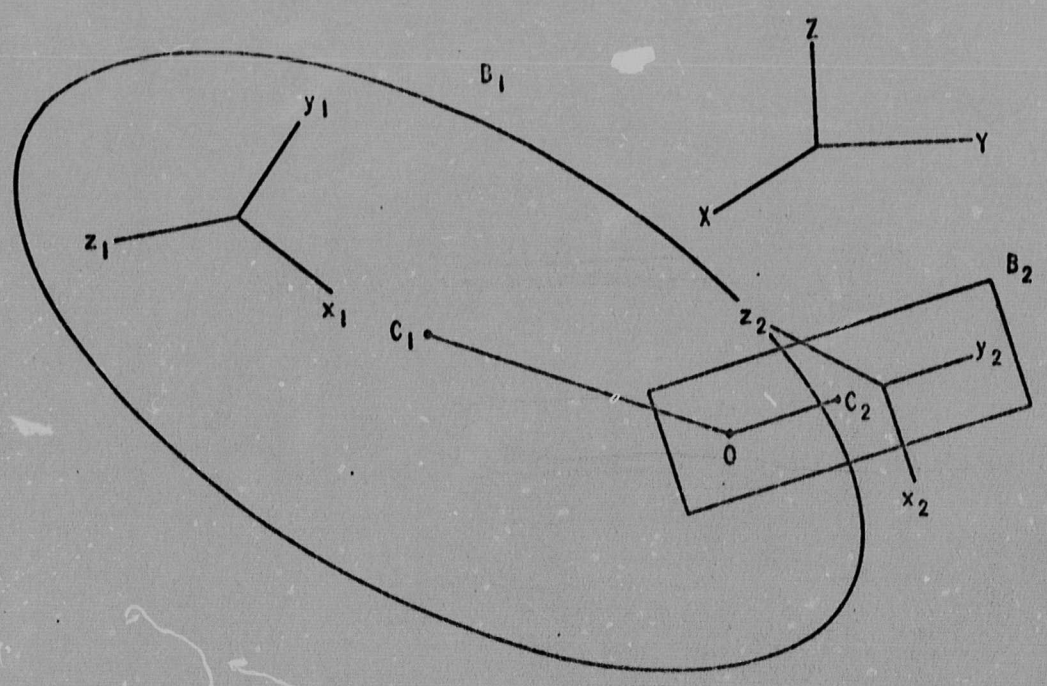

Figure I
The dynamical model

The telescope optical axis is parallel to y_2, and the two gimbal axes are respectively parallel to x_1 and z_2, γ_1 and γ_2 being the corresponding gimbal rotation angles; $x_1y_1z_1$ and $x_2y_2z_2$ are aligned when $\gamma_1=\gamma_2=0$. Let the gimbal axes intersect at 0. The location of C_1, the mass center of B_1, relative to 0 is specified by p_1, p_2, and p_3, the $x_1y_1z_1$ measure numbers* of the relative position vector; likewise, q_1, q_2, q_3 are the measure numbers with respect to $x_2y_2z_2$ of the location of C_2 relative to 0.

The orientation of B_2 with respect to the inertially fixed axes XYZ is specified by means of the angles ϕ,θ, and ψ, generated as follows: initially align $x_2y_2z_2$ with XYZ; rotate $x_2y_2z_2$ about z_2 by an amount ψ; follow with a rotation about y_2 of amount θ; then perform a rotation of magnitude ϕ about x_2, bringing $x_2y_2z_2$ into its final position. The foregoing procedure is sometimes known as a 3, 2, 1 Euler angle sequence involving the angles ψ,θ, and ϕ, respectively.

Linearized Equations

The equations of motion from Reference 2 are first linearized in $\phi,\theta,\psi,\gamma_1,\gamma_2$ and their derivatives**; the result may be written in the form

$$(A_1 + A_2)\,\ddot{u} = G_1(t) + G_2(t) + G_3'(t) \qquad (I\text{-}1)$$

---

* A measure number is simply the dot product of a vector of interest (e.g., the relative position vector) with unit vector having the indicated direction (e.g., parallel to x_1). The term "measure number" is distinguished from the term "component" in that the former is a scalar, whereas the latter is a vector.

**Linearization is a suitable approximation here because $\phi,\theta,\psi,\gamma_1,\gamma_2$ may be chosen so that they remain small and it is reasonable to assume that their derivatives also remain small.

in which A_1 and A_2 are 5x5 constant matrices, u is a 5x1 vector whose elements are $\phi, \theta, \psi, \gamma_1, \gamma_2$, respectively, and G_1, G_2, G_3 are 5x1 vectors. Matrix A_1 is symmetric, and it depends on m_1 and m_2, the masses of B_1 and B_2, respectively:

$$A_1 = \frac{m_1 m_2}{m_1+m_2} \begin{bmatrix} s_2^2+s_3^2 & -s_1s_2 & -s_1s_3 & -p_2s_2-p_3s_3 & p_1s_3 \\ -s_1s_2 & s_1^2+s_2^2 & -s_2s_3 & p_2s_1 & p_2s_3 \\ -s_1s_3 & -s_2s_3 & s_1^2+s_2^2 & p_3s_1 & -p_1s_1-p_2s_2 \\ -p_2s_2-p_3s_3 & p_2s_1 & p_3s_1 & p_2^2+p_3^2 & -p_1p_3 \\ p_1s_3 & p_2s_3 & -p_1s_1-p_2s_2 & -p_1p_3 & p_1^2+p_2^2 \end{bmatrix} \quad (I-2)$$

where

$$s_i = p_i - q_i \quad , \quad i = 1, 2, 3 \quad (I-3)$$

Matrix A_2 is also symmetric, and it depends on the centroidal moments of inertia I_i, J_i, K_i, i=1, 2, of B_i about the axes $x_i y_i z_i$, respectively (It is assumed here that the principal axes are sufficiently well aligned with $x_i y_i z_i$ that the products of inertia may be neglected).

$$A_2 = \begin{bmatrix} I_1+I_2 & 0 & 0 & -I_1 & 0 \\ 0 & J_1+J_2 & 0 & 0 & 0 \\ 0 & 0 & K_1+K_2 & 0 & -K_1 \\ -I_1 & 0 & 0 & I_1 & 0 \\ 0 & 0 & -K_1 & 0 & K_1 \end{bmatrix} \quad (I-4)$$

Column vectors G_1, G_2, G_3' account for the forces and torques exerted on B_1 and B_2. Let $\underline{F}_i$, i=1, 2 denote the force acting on B_i,* and let F_{ix}, F_{iy}, F_{iz} be the measure numbers of $\underline{F}_i$ with respect to x_i, y_i, z_i. The torque acting on B_1 is $\underline{T}_1-\underline{T}_c-\underline{T}_g'$, and that acting on B_2 is $\underline{T}_2+\underline{T}_g'$, where $\underline{T}_c$ is the torque exerted on the CMGs by the spacecraft, $\underline{T}_g$ is the torque exerted on B_2 by B_1 about the gimbal axes, and $\underline{T}_1$ and $\underline{T}_2$ are the torques exerted on B_1 and B_2, respectively, due to gravitational, aerodynamic, and crew motion disturbances. Let the measure numbers of $\underline{T}_1-\underline{T}_c-\underline{T}_g'$ with respect to x_1, y_1, z_1 be donoted by T_{1x}', T_{1y}', T_{1z}, respectively. Likewise, let T_{2x}, T_{2y}, T_{2z} denote the measure numbers of $\underline{T}_2+\underline{T}_g'$ with respect to x_2, y_2, z_2. Matrices G_1, G_2, G_3' may now be defined:

$$G_1(t) = \frac{1}{1+(m_1/m_2)}\begin{bmatrix} -F_{1y}s_3+F_{1z}s_2 \\ F_{1x}s_3-F_{1z}s_1 \\ -F_{1x}s_2+F_{1y}s_1 \\ F_{1y}p_3-F_{1z}p_2 \\ F_{1x}p_2-F_{1y}p_1 \end{bmatrix} \qquad (I\text{-}5)$$

$$G_2(t) = \frac{1}{1+(m_2/m_1)}\begin{bmatrix} F_{2y}s_3-F_{2z}s_2 \\ -F_{2x}s_3+F_{2z}s_1 \\ F_{2x}s_2-F_{2y}s_1 \\ -F_{2y}p_3+F_{2z}p_2 \\ -F_{2x}p_2+F_{2y}p_1 \end{bmatrix} \qquad (I\text{-}6)$$

---

*The forces and torques $\underline{F}_1$, $\underline{F}_2$, $\underline{T}_1$, $\underline{T}_2$, $\underline{T}_c$, and $\underline{T}_g'$ are defined in detail in Reference 2, Section 3.2.

$$G_3'(t) = \begin{bmatrix} T_{1x}' + T_{2x} \\ T_{1y}' + T_{2y} \\ T_{1z}' + T_{2z} \\ -T_{1x}' \\ -T_{1z}' \end{bmatrix} \qquad \text{(I-7)}$$

Control and Disturbance Torques

If the CMG gimbal angles are small, the CMG control system behaves essentially as a linear feedback control, and $\underline{T}_c$ may then be expressed as a linear combination of carrier attitude error and error rate. To this end, let the attitude of the carrier relative to the inertially fixed axes XYZ be specified in terms of a 3, 2, 1 Euler angle sequence involving the angles ψ', θ', ϕ'. Orient the XYZ axes such that they are aligned with the $x_1 y_1 z_1$ axes when the carrier is in the desired orientation. Now, the ATM vernier gimbal angles γ_1 and γ_2 are limited to small values by mechanical stops, and the PCS is designed to keep excursions of the carrier from its desired attitude small. Within the approximation of the linearization carried out previously, we thus have that

$$\phi' = \phi - \gamma_1 \quad , \quad \theta' = \theta \quad , \quad \psi' = \psi - \gamma_2 \qquad \text{(I-8)}$$

Therefore, for small CMG gimbal angles, $\underline{T}_c$ has measure numbers

$$K_{rx}(\dot{\phi} - \dot{\gamma}_1) + K_{ex}(\phi - \gamma_1)$$

$$K_{ry}\,\dot{\theta} + K_{ey}\,\theta$$

$$K_{rz}(\dot{\psi} - \dot{\gamma}_2) + K_{ez}(\psi - \gamma_2)$$

with respect to $x_1 y_1 z_1$. The quantities denoted by K_{rx}, K_{ry}, K_{rz} are the rate feedback gains and K_{ex}, K_{ey}, K_{ez} denote the error feedback gains.

Telescope attitude is maintained by a linear feedback system called the Experiment Pointing Control (EPC) that ideally applies torques $\underline{T}_g$ about the gimbal axes in response to a linear combination of telescope attitude error and error rate. In reality, because of torquer breakout torque, the torque commanded is not the torque actually delivered. Let $\tau(i)$ be a function that defines the torquer characteristic, i.e., the actual torque resulting from a commanded torque i; τ is not necessarily a function of i alone. The actual torquer output, $\underline{T}_g$ thus has measure numbers

$$\tau(-K_{r1}\dot{\phi} - K_{e1}\phi)$$

$$\tau(-K_{r2}\dot{\psi} - K_{e2}\psi)$$

with respect to x_1 and z_2.

Crew motion disturbances account for larger peak pointing error than other sources of disturbance, such as gravitational or aerodynamic effects. For this reason, the latter effects are neglected; vectors $\underline{F}_1$ and $\underline{T}_1$ then arise solely from crew motion disturbances, and $\underline{F}_2=\underline{T}_2=0$.

It is now possible to write equation (I-1) in a form more useful for our purposes:

$$A\ddot{u} + K_r\dot{u} + K_e u = G_1(t) + G_3(t) + H \qquad (I\text{-}9)$$

Here A is simply the sum of matrices A_1 and A_2:

$$A = \begin{bmatrix} I_1+I_2+m(s_2^2+s_3^2) & -ms_1s_2 & -ms_1s_3 & -I_1-m(p_2s_2+p_3s_3) & mp_1s_3 \\ -ms_1s_2 & J_1+J_2+m(s_1^2+s_3^2) & -ms_2s_3 & mp_2s_1 & mp_2s_3 \\ -ms_1s_3 & -ms_2s_3 & K_1+K_2+m(s_1^2+s_2^2) & mp_3s_1 & -K_1-m(p_1s_1+p_2s_2) \\ -I_1-m(p_2s_2+p_3s_3) & mp_2s_1 & mp_3s_1 & I_1+m(p_2^2+p_3^2) & -mp_1p_3 \\ mp_1s_3 & mp_2s_3 & -K_1-m(p_1s_1+p_2s_2) & -mp_1p_3 & K_1+m(p_1^2+p_2^2) \end{bmatrix} \quad (I-10)$$

where

$$m = \frac{m_1 m_2}{m_1+m_2} \quad (I-11)$$

The 5x5 matrices K_r and K_e are composed of the control system gains:

$$K_r = \begin{bmatrix} K_{rx} & 0 & 0 & -K_{rx} & 0 \\ 0 & K_{ry} & 0 & 0 & 0 \\ 0 & 0 & K_{rz} & 0 & -K_{rz} \\ -K_{rx}+K_{r1} & 0 & 0 & K_{rx} & 0 \\ 0 & 0 & -K_{rz}+K_{r2} & 0 & K_{rz} \end{bmatrix} \quad (I-12)$$

$$K_e = \begin{bmatrix} K_{ex} & 0 & 0 & -K_{ex} & 0 \\ 0 & K_{ey} & 0 & 0 & 0 \\ 0 & 0 & K_{ez} & 0 & -K_{ez} \\ -K_{ex}+K_{e1} & 0 & 0 & K_{ex} & 0 \\ 0 & 0 & -K_{ez}+K_{e2} & 0 & K_{ez} \end{bmatrix} \quad (I-13)$$

Let T_{1x}, T_{1y}, T_{1z} denote the measure numbers with respect to x_1, y_1, z_1 of the crew disturbance torque $\underline{T}_1$ when the crew disturbance force $\underline{F}_1$ is applied to B_1 at C_1. Then

$$G_3(t) = \begin{bmatrix} T_{1x} \\ T_{1y} \\ T_{1z} \\ T_{1x} \\ -T_{1z} \end{bmatrix} \qquad \text{(I-14)}$$

The 5x1 vector H accounts for the gimbal suspension torques $\underline{T}_g'-\underline{T}_g$ that are exerted between B_1 and B_2 about axes x_1 and z_2 in addition to the EPC torque $\underline{T}_g$. If T_{g1} and T_{g2} are the x_1 and z_2 measure numbers of $\underline{T}_g'-\underline{T}_g$, then

$$H = \begin{bmatrix} 0 \\ 0 \\ 0 \\ T_{g1} \\ T_{g2} \end{bmatrix} \qquad \text{(I-15)}$$

It should be noted that the torquer characteristic has been neglected in (I-9), i.e., it is assumed that $\tau(x)=x$. This function will be incorporated into the equations later.

Single-Axis Equations

Solution of (I-9) would be facilitated if these five differential equations could be written as independent (uncoupled) equations. Inspection of matrices K_r and K_e reveals that although these matrices do contribute to the dependence of

the equations (because of the non-zero off-diagonal elements), the contributions are independent about the x axis (i.e., in the variables $u_1=\phi$ and $u_4=\gamma_1$), the y axis ($u_2=\theta$), and the z axis ($u_3=\psi$ and $u_5=\gamma_2$). Matrix A clearly does not possess this single-axis independence, but it will now be shown that those elements of A corresponding to the zero elements of K_r and K_e are small in comparison to those elements of A corresponding to the non-zero elements of K_r and K_e.

It is necessary to choose numerical data for the vehicle in order to evaluate A; the data used are those for the current ATM, as obtained from Reference 10.

$m_1 = 3367$ slugs $\qquad m_2 = 171$ slugs

$I_1 = 5.771\times10^5$ slug-ft^2 $\qquad I_2 = 2.342\times10^3$ slug-ft^2

$J_1 = 3.649\times10^6 \qquad J_2 = 1.076\times10^3$

$K_1 = 3.737\times10^6 \qquad K_2 = 2.363\times10^3$

$s_1-p_1=-13.86$ ft, $s_2-p_2=-22.98$ ft, $s_3-p_3=-.16$ ft

For these data

$$A = \begin{bmatrix} 0.7 & -.05 & -.0004 & -0.7 & .0004 \\ -.05 & 4. & -.0006 & .05 & .0006 \\ -.0004 & -.0006 & 4. & .0004 & -4. \\ -0.7 & .05 & .0004 & 0.7 & -.0004 \\ .0004 & .0006 & -4. & -.0004 & 4. \end{bmatrix} \times10^6 \text{ slug-ft}^2$$

If the elements of A whose value is less than 10^5 slug-ft^2 are neglected, then A assumes the same form, i.e., has zeros in the same locations, as K_r and K_e. Equations (I-9) may now be written as three independent sets of equations, one set for each axis:

$$[I_1+I_2+m(s_2^2+s_3^2)]\ddot{\phi} - [I_1+m(p_2s_2+p_3s_3)]\ddot{\gamma}_1 + K_{rx}\dot{\phi} - K_{rx}\dot{\gamma}_1$$

$$+ K_{ex}\phi - K_{ex}\gamma_1 = M(-F_{1y}s_3+F_{1z}s_2) + T_{1x} \quad \text{(I-16)}$$

$$-[I_1+m(p_2s_2+p_3s_3)]\ddot{\phi} + [I_1+m(p_2^2+p_3^2)]\ddot{\gamma}_1 + (-K_{rx}+K_{r1})\dot{\phi} + K_{rx}\dot{\gamma}_1$$

$$+ (-K_{ex}+K_{e1})\phi + K_{ex}\gamma_1 = M(F_{1y}p_3-F_{1z}p_2) - T_{1x} + T_{g1} \quad \text{(I-17)}$$

$$[J_1+J_2+m(s_1^2+s_3^2)]\ddot{\theta} + K_{ry}\dot{\theta} + K_{ey}\theta = M(F_{1x}s_3-F_{1z}s_1) + T_{1y} \quad \text{(I-18)}$$

$$[K_1+K_2+m(s_1^2+s_2^2)]\ddot{\psi} - [K_1+m(p_1s_1+p_2s_2)]\ddot{\gamma}_2 + K_{rz}\dot{\psi} - K_{rz}\dot{\gamma}_2$$

$$+ K_{ez}\psi - K_{ez}\gamma_2 = M(-F_{1x}s_2+F_{1y}s_1) + T_{1z} \quad \text{(I-19)}$$

$$-[K_1+m(p_1s_1+p_2s_2)]\ddot{\psi} + [K_1+m(p_1^2+p_2^2)]\ddot{\gamma}_2 + (-K_{rz}+K_{rz})\dot{\psi} + K_{rz}\dot{\gamma}_2$$

$$+ (-K_{ez}+K_{e2})\psi + K_{ez}\gamma_2 = M(F_{1x}p_2-F_{1y}p_1) - T_{1z} + T_{g2} \quad \text{(I-20)}$$

where

$$M = \frac{1}{1+(m_1/m_2)} \quad \text{(I-21)}$$

For convenience let

$$a_1 = I_1 + I_2 + m(s_2^2+s_3^2) \quad , \quad b_1 = -I_1 - m(p_2s_2+p_3s_3)$$

$$a_2 = -I_1 - m(p_2s_2+p_3s_3) \quad , \quad b_2 = I_1 + m(p_2^2+p_3^2)$$

$$a_3 = K_{rx} \quad , \quad b_3 = -K_{rx} + K_{rl}$$

$$a_4 = -K_{rx} \quad , \quad b_4 = K_{rx}$$

$$a_5 = K_{ex} \quad , \quad b_5 = -K_{ex} + K_{el}$$

$$a_6 = -K_{ex} \quad , \quad b_6 = K_{ex}$$

$$a_7 = M(-F_{1y}s_3+F_{1z}s_2) + T_{1x} \quad , \quad b_7 = M(F_{1y}p_3-F_{1z}p_2) - T_{1x} + T_{g1} \qquad (I-22)$$

(Notice that $a_1,\ldots, a_6$, $b_1,\ldots,b_6$ are constants, whereas a_7 and b_7 are in general variable.) The x-axis equations, (I-16) and (I-17), may now be written

$$a_1 \ddot{\phi} + a_2 \ddot{\gamma}_1 + a_3 \dot{\phi} + a_4 \dot{\gamma}_1 + a_5 \phi + a_6 \gamma_1 = a_7 \qquad (I-23)$$

$$b_1 \ddot{\phi} + b_2 \ddot{\gamma}_1 + b_3 \dot{\phi} + b_4 \dot{\gamma}_1 + b_5 \phi + o_6 \gamma_1 = b_7 \qquad (I-24)$$

By appropriate change of variables and redefinition of $a_1,\ldots, a_7$, $b_1,\ldots, b_7$, the z-axis equations, (I-19) and (I-20), may also be written in the form (I-23), (I-24), and hence the techniques to be developed to deal with (I-23), (I-24) may be applied to either the x-axis or the z-axis equations.

By further approximation, equation (I-23) may be expressed solely in terms of the variable ϕ'. To this end, use (I-8) to eliminate ϕ from (I-23):

$$a_1 \ddot{\phi}' + (a_1+a_2) \ddot{\gamma}_1 + a_3 \dot{\phi}' + (a_3+a_4) \dot{\gamma}_1 + a_5 \phi' + (a_5+a_6) \gamma_1 = a_7 \qquad (I-25)$$

Note from (I-22) that $a_3+a_4=a_5+a_6=0$, and rewrite (I-25) as

$$-a_2 \ddot{\phi}' + (a_1+a_2)(\ddot{\phi}'+\ddot{\gamma}_1) + a_3 \dot{\phi}' + a_5 \phi' = a_7 \qquad \text{(I-26)}$$

If the carrier is "reasonably large" compared to the telescope, then

$$|a_1+a_2| << |a_2|$$

and if the control system is properly designed, then

$$|\ddot{\phi}'+\ddot{\gamma}_1| = |\ddot{\phi}| << |\ddot{\phi}'|$$

It follows that the second term of (I-26) may be neglected when compared to the first term. The simplified carrier x-axis equation is thus

$$[I_1+m(p_2s_2+p_3s_3)]\ddot{\phi}' + K_{rx}\dot{\phi}' + K_{ex}\phi' = M(-F_{1y}s_3+F_{1z}s_2) + T_{1x} \qquad \text{(I-27)}$$

and the corresponding approximate carrier z-axis equation is

$$[K_1+m(p_1s_1+p_2s_2)]\ddot{\psi}' + K_{rz}\dot{\psi}' + K_{ez}\psi' = M(-F_{1x}s_2+F_{1y}s_1) + T_{1z} \qquad \text{(I-28)}$$

The two preceding equations may be used to obtain the approximate motion of the carrier independently of the telescope motion. Although it would be convenient to have similar simplified equations that describe the telescope motion independently of the carrier motion, such equations would not be descriptive of reality, since the telescope motion does depend intimately on the carrier motion. Equations expressing the influence of the carrier motion on motions of the telescope may be obtained by adding (I-23) and (I-24):

$$(a_1+b_1)\ddot{\phi}+(a_2+b_2)\ddot{\gamma}_1+(a_3+b_3)\dot{\phi}+(a_4+b_4)\dot{\gamma}_1+(a_5+b_5)\phi+(a_6+b_6)\gamma_1=a_7+b_7 \quad \text{(I-29)}$$

Use of (I-22) yields

$$[I_2-m(q_2s_2+q_3s_3)]\ddot{\phi} + m(p_2q_2+p_3q_3)\ddot{\gamma}_1 + K_{r1}\dot{\phi} + K_{e1}\dot{\phi}$$

$$= M(F_{1y}q_3-F_{1z}q_2) + T_{g1} \quad \text{(I-30)}$$

Rearrangement and incorporation of the torquer characteristic give the desired expression:

$$[I_2-m(q_2s_2+q_3s_3)]\ddot{\phi}-\tau(-K_{r1}\dot{\phi}-K_{e1}\phi) = -m(p_2q_2+p_3q_3)\ddot{\gamma}_1$$

$$+M(F_{1y}q_3-F_{1z}q_2) + T_{g1} \quad \text{(I-31)}$$

The corresponding equation for the z-axis is

$$[K_2-m(q_1s_1+q_2s_2)]\ddot{\psi}-\tau(-K_{r2}\dot{\psi}-K_{e2}\psi) = -m(p_1q_1+p_2q_2)\ddot{\gamma}_2$$

$$+M(F_{1x}q_2-F_{1y}q_1) + T_{g2} \quad \text{(I-32)}$$

Equations (I-31) and (I-32) indicate clearly that telescope attitude is influenced by carrier angular acceleration ($\ddot{\gamma}_1$ and $\ddot{\gamma}_2$), by loads applied to the carrier (F_{1x}, F_{1y}, F_{1z}), and by torques imparted by the gimbal suspension system (T_{g1} and T_{g2}). The reader should also observe that if three conditions are all met, namely

1) the telescope mass center, C_2, coincides with the intersection of the gimbal axes, 0, i.e., $q_1=q_2=q_3=0$

2) there are no gimbal suspension torques, i.e., $T_{g1}=T_{g2}=0$

3) the torquers have an ideal characteristic, i.e., $\tau(x)=x$

then (I-31) and (I-32) reduce to

$$I_2\ddot{\phi}+K_{r1}\dot{\phi}+K_{e1}\phi=0 \quad , \quad K_2\ddot{\psi}+K_{r2}\dot{\psi}+K_{e2}\psi=0 \qquad \text{(I-33)}$$

whose solutions decay exponentially provided that $K_{r1}>0$, $K_{r2}>0$. It should also be noticed that we now have a means for obtaining an approximate analytical solution to the equations of motion when $\tau(x)=x$; following is the sequence to be followed in obtaining a solution:*

1. Prescribe the crew motion disturbances $\underline{F}_1$ and $\underline{T}_1$ as functions of time.

2. Solve the linear, second order, constant coefficient equations (I-27), (I-18), (I-28) for the carrier motion $\phi'(t)$, $\theta(t)$, $\psi'(t)$.

3. Recall that in general $|\phi|<<|\phi'|$, $|\psi|<<|\psi'|$, and thus $\gamma_1\simeq-\phi'$, $\gamma_2\simeq-\psi'$.

4. Prescribe the gimbal suspension torques T_{g1} and T_{g2} as functions of time or gimbal angle.

5. Solve the linear, second order, constant coefficient equations (I-31) and (I-32) for the telescope motion $\phi(t)$ and $\psi(t)$ by using $\gamma_1(t)$ and $\gamma_2(t)$ obtained in steps 2 and 3.

---

*The author has used this method to obtain the x-axis telescope motion for the case when the crew motion is a square wave function of time and T_{g1} is linearly dependent on γ_1.

APPENDIX II

Means of Reducing Torquer Breakout Torque*

The ATM gimbal torquers employ a permanent magnet stator and a rotor with windings on a core of magnetically soft material. Breakout torque is primarily due to magnetic hysteresis in the core material.**

Since hysteresis loss generally varies as the 1.6 to 2.0 power of flux density, one of the most effective ways of reducing breakout torque is to reduce rotor flux density. This may be done simply by partially demagnetizing the stator, and although this results in a reduction of peak torque proportional to the reduction in flux density, the ATM torquers are currently capable of producing more torque than is required anyway. As an example, assume that we will accept a reduction in peak torque from the 1" ft-lb (for both torquers) used in the ATM to the quite adequate value of 1 ft-lb. The ATM torquers obey a 1.8 power relationship between flux density and hysteresis drag,** and thus breakout torque reduces from .08 ft-lb to 6.9×10^{-4} ft-lb as peak torque is decreased to 1/14 of its original value; if one assumes a more conservative 1.6 power relationship, breakout torque becomes .0012 ft-lb, still well below the value consistent with .01 arc second pointing accuracy.

The scheme just described appears to be a quite satisfactory means for reducing breakout torque since it is simple and since the loss incurred in peak torque is not detrimental to control system performance. However, if one will accept an increase in torquer size, one can maintain peak torque while reducing breakout torque, this being possible because of the previously mentioned facts that breakout torque varies as the 1.6 to 2.0 power of flux density, whereas peak torque varies only linearly with flux density. If one assumes a 1.8 power relationship between flux density and hysteresis drag, a 10:1 reduction in drag (.08 to .008 ft-lb for the ATM torquers) can be achieved by increasing torquer weight by a factor of about 18,

---

* This material is the result of discussions with G. M. Anderson of Bellcomm and S. Noodleman of Inland Motor Corporation, whose help is gratefully acknowledged.

** See Reference 11.

i.e., one could increase both torquer diameter and length by a factor of about 2.6, for example. Assuming the conservative 1.6 power relationship, we find that a 10:1 reduction in drag results from a 1:46 increase in torquer weight, i.e., a 1:3.6 increase in both diameter and length, for example.

Breakout torque can also be reduced by using a rotor core material having less hysteresis loss than the material (Jalox) used in the ATM torquers. Inland Motor Corporation has suggested Mumetal for this application,* since it has only about 5 percent of the hysteresis loss of Jalox (at the same flux density).

---

* See Reference 11.

APPENDIX III

Telescope Attitude Expressions for Large Gimbal Angles

Let $\underline{i}_I$, $\underline{j}_I$, $\underline{k}_I$ denote a set of right handed, mutually orthogonal unit vectors fixed in an inertial reference frame, and let $\underline{i}_2$, $\underline{j}_2$, $\underline{k}_2$ be a set of right handed unit vectors respectively parallel to $x_2y_2z_2$; quantities ϕ', θ', ψ', γ_1, and γ_2 are defined as before.† The two sets of unit vectors may be related by the transformation T,

$$\begin{bmatrix} \underline{i}_2 \\ \underline{j}_2 \\ \underline{k}_2 \end{bmatrix} = T \begin{bmatrix} \underline{i}_I \\ \underline{j}_I \\ \underline{k}_I \end{bmatrix}$$

$$T = \begin{bmatrix} (c\gamma_2 - \psi' c\gamma_1 s\gamma_2 + \theta' s\gamma_1 s\gamma_2) & (\psi' c\gamma_2 + c\gamma_1 s\gamma_2 - \phi' s\gamma_1 s\gamma_2) & (-\theta' c\gamma_2 + \phi' c\gamma_1 s\gamma_2 + s\gamma_1 s\gamma_2) \\ (-s\gamma_2 - \psi' c\gamma_1 c\gamma_2 + \theta' s\gamma_1 c\gamma_2) & (-\psi' s\gamma_2 + c\gamma_1 c\gamma_2 - \phi' s\gamma_1 c\gamma_2) & (\theta' s\gamma_2 + \phi' c\gamma_1 c\gamma_2 + s\gamma_1 c\gamma_2) \\ (\psi' s\gamma_1 + \theta' c\gamma_1) & (-s\gamma_1 - \phi' c\gamma_1) & (-\phi' s\gamma_1 + c\gamma_1) \end{bmatrix}$$

Here the notation $c\gamma_2 = \cos\gamma_2$, etc., is used, and it is assumed that ϕ', θ', ψ' are small (consistent with the assumptions made in the carrier modal analysis). We define $\underline{i}_2^*$, $\underline{j}_2^*$, $\underline{k}_2^*$ to be a set of inertially fixed unit vectors that are respectively parallel to $\underline{i}_I$, $\underline{j}_I$, $\underline{k}_I$ when $\phi' = \theta' = \psi' = 0$, $\gamma_1 = \gamma_1^*$, $\gamma_2 = \gamma_2^*$, and we introduce the transformation

---

†Axes $x_2y_2z_2$ and gimbal angles are defined in the Problem Statement, Appendix I; and ϕ', θ', ψ' are defined in Control and Disturbance Torques, Appendix I.

$$T^* = \begin{bmatrix} c\gamma_2^* & c\gamma_1^* s\gamma_2^* & s\gamma_1^* s\gamma_2^* \\ -s\gamma_2^* & c\gamma_1^* c\gamma_2^* & s\gamma_1^* c\gamma_2^* \\ 0 & -s\gamma_1^* & c\gamma_1^* \end{bmatrix}$$

which satisfies the relationship

$$\begin{bmatrix} \underline{i}_2^* \\ \underline{j}_2^* \\ \underline{k}_2^* \end{bmatrix} = T^* \begin{bmatrix} \underline{i}_I \\ \underline{j}_I \\ \underline{k}_I \end{bmatrix}$$

This transformation is orthogonal, and thus the desired relationship is obtained:

$$\begin{bmatrix} \underline{i}_2 \\ \underline{j}_2 \\ \underline{k}_2 \end{bmatrix} = T\, T^{*T} \begin{bmatrix} \underline{i}_2^* \\ \underline{j}_2^* \\ \underline{k}_2^* \end{bmatrix}$$

The vectors $\underline{i}_2^*$, $\underline{j}_2^*$, $\underline{k}_2^*$ define the desired attitude of the telescope, and it is assumed that the telescope makes only small excursions from its desired attitude. Under these circumstances, the telescope attitude may be expressed in terms of small rotations ϕ, θ, ψ about $\underline{i}_2^*$, $\underline{j}_2^*$, $\underline{k}_2^*$, respectively, and the unit vectors may be related approximately by

$$\begin{bmatrix} \underline{i}_2 \\ \underline{j}_2 \\ \underline{k}_2 \end{bmatrix} = \begin{bmatrix} 1 & \psi & -\theta \\ -\psi & 1 & \phi \\ \theta & -\phi & 1 \end{bmatrix} \begin{bmatrix} \underline{i}_2^* \\ \underline{j}_2^* \\ \underline{k}_2^* \end{bmatrix}$$

An expression for ϕ is obtained as the average of the two elements of TT^{*T} corresponding to the locations of ϕ in above equation.

$$\phi = [(TT^{*T})_{23} - (TT^{*T})_{32}]/2$$

$$= \frac{1}{2}[\phi'(c\gamma_2+c\gamma_2^*)\cos(\gamma_1-\gamma_1^*) + \theta'(c\gamma_1^* s\gamma_2 + s\gamma_2^* c\gamma_1)$$

$$+ \psi'(s\gamma_1^* s\gamma_2 + s\gamma_2^* s\gamma_1) + (c\gamma_2+c\gamma_2^*)\sin(\gamma_1-\gamma_1^*)]$$

Similarly, an expression for ψ is obtained.

$$\psi = [(TT^{*T})_{12} - (TT^{*T})_{21}]/2$$

$$= \frac{1}{2}\{-\phi' \sin(\gamma_1-\gamma_1^*)\sin(\gamma_2-\gamma_2^*) - \theta'(s\gamma_1+s\gamma_1^*)\cos(\gamma_2-\gamma_2^*$$

$$+ \psi'(c\gamma_1+c\gamma_1^*)\cos(\gamma_2-\gamma_2^*) + [1+\cos(\gamma_1-\gamma_1^*)]\sin(\gamma_2-\gamma_2^*)\}$$

References

1. Chubb, W. B., Schultz, D. N., and Seltzer, S. M., "Attitude Control and Precision Pointing of the Apollo Telescope Mount," Journal of Spacecraft, Vol. 5, pp. 896-903 (August 1968).

2. Smith, P. G., "A Mathematical Model for Simulation of the Apollo Telescope Mount Pointing Control System," Bellcomm TR-68-620-1, May 8, 1968.

3. Cornelius, C. S. (MSFC), Personal Communication, May 21, 1968.

4. Strasser, J. A., "Flight Hardware for ATM Control System Takes Shape at MSFC," Aerospace Technology, June 3, 1968, p. 43.

5. (Available from two sources) (1) Kroll, G. A., "Preliminary Vibration Analysis of the S-IVB Orbital Workshop Cluster," MSFC Memorandum R-P&VE-SLS-68-13, May 15, 1968; (2) Pack, Homer, "Preliminary Vibration Data of the AAP Cluster (Configuration ___)," MSFC Memorandum R-AERO-DD-99-68, April 24, 1968.

6. Skelton, R. E. (Sperry-Rand, Huntsville), Personal Communication, November 7, 1968.

7. Hough, W. W. and Schmuecker, J. D., "Mariner-Mars Inertial Properties Determination and Midcourse Motor Alignment," Jet Propulsion Laboratory TR 32-852, May 15, 1968, pp. 30-31.

8. "The OAO in Association with a Manned Space Station," Vol.III, Grumman Aircraft Engineering Corporation, ASR 252B-1, June 1965, pp. 45-53.

9. "Princeton Advanced Satellite Study," Vol. III, Perkin-Elmer Corporation Report No. 8346 (III), pp. 3-92 through 3-94.

10. Aberg, J. O., "Mass Characteristics for the Cluster Mission," MSFC Memorandum R-P&VE-VAW-68-110, August 26, 1968.

11. Smith, P. G., "Trip Report - Visit to Inland Motor Corporation to Discuss Torquer Design," Bellcomm Memorandum for File, January 15, 1969.

END